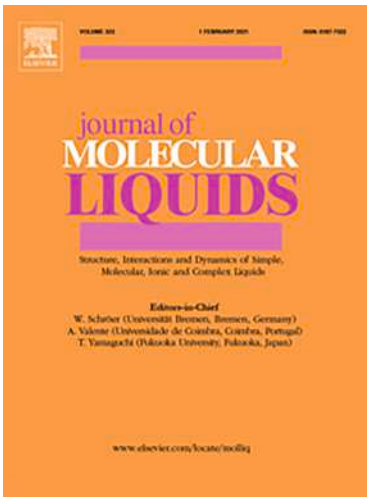

Computational Prediction of Potential Drug-like Compounds from *Cannabis sativa* Leaf Extracts Targeted towards Alzheimer Therapy

Adewale Oluwaseun Fadaka, Odunayo Anthonia Taiwo, Oluwatosin Adebisi Dosumu, Oluwafemi Paul Owolabi, Adebola Busola Ojo, Nicole Remaliah Samantha Sibuyi, Samee Ullah, Ashwil Klein, Abram Madimabe Madiehe, Mervin Meyer, Oluwafemi Adeleke Ojo

PII: S0167-7322(22)00931-X
DOI: https://doi.org/10.1016/j.molliq.2022.119393
Reference: MOLLIQ 119393

To appear in: *Journal of Molecular Liquids*

Received Date: 4 October 2021
Revised Date: 11 May 2022
Accepted Date: 12 May 2022

Please cite this article as: A. Oluwaseun Fadaka, O. Anthonia Taiwo, O. Adebisi Dosumu, O. Paul Owolabi, A. Busola Ojo, N. Remaliah Samantha Sibuyi, S. Ullah, A. Klein, A. Madimabe Madiehe, M. Meyer, O. Adeleke Ojo, Computational Prediction of Potential Drug-like Compounds from *Cannabis sativa* Leaf Extracts Targeted towards Alzheimer Therapy, *Journal of Molecular Liquids* (2022), doi: https://doi.org/10.1016/j.molliq.2022.119393

Computational Prediction of Potential Drug-like Compounds from *Cannabis sativa* Leaf Extracts Targeted towards Alzheimer Therapy

Adewale Oluwaseun Fadaka[1,2]*, Odunayo Anthonia Taiwo[3,4], Oluwatosin Adebisi Dosumu[4], Oluwafemi Paul Owolabi[4], Adebola Busola Ojo[5], Nicole Remaliah Samantha Sibuyi[2], Samee Ullah[6], Ashwil Klein[7], Abram Madimabe Madiehe[2,8], Mervin Meyer[2], Oluwafemi Adeleke Ojo[9]*

[1]Department of Anesthesia, Division of Pain Management, Cincinnati Children's Hospital Medical Center, Cincinnati, Ohio 45229.
[2]Department of Science and Innovation/Mintek Nanotechnology Innovation Centre, Biolabels Node, Department of Biotechnology, Faculty of Natural Sciences, University of the Western Cape, Bellville, South Africa
[3]Department of Biochemistry, Chrisland University, Abeokuta, Nigeria
[4]Department of Biochemistry, Federal University of Agriculture, Abeokuta, Nigeria
[5]Department of Biochemistry, Ekiti State University, Ado-Ekiti, Nigeria
[6]National Institute of Health, Park Road, Chak Shahzad, Islamabad-45500
[7]Plant Omics Laboratory, Department of Biotechnology, Faculty of Natural Sciences, University of the Western Cape, Private Bag X17, Bellville, 7535, Cape Town, South Africa
[8]Nanobiotechnology Research Group, Department of Biotechnology, Faculty of Natural Sciences, University of the Western Cape, Bellville, South Africa
[9]Phytomedicine, Natural Products, and Molecular Toxicology Research Group, Department of Biochemistry, Landmark University, Omu-Aran, Nigeria

***Corresponding authors**: AO Fadaka: Adewale.fadaka@cchmc.org, afadaka@uwc.ac.za; Tel: +15137642728
OA Ojo: oluwafemiadeleke08@gmail.com; Tel: +2347037824647

Abstract

This study was aimed at evaluating the inhibitory effects of the phytochemicals from the *Cannabis sativa* (Cannabis) leaf extracts against Alzheimer's disease (AD) protein targets. Twelve compounds derived from the *Cannabis sativa* leaf extracts were evaluated as potential inhibitors of acetylcholinesterase (AChE), dopa decarboxylase (DDC), serotonin receptor 2C (HTR2C) and monoamine oxidase (MAO). Ligand-based and receptor-ligand complex were used to derive the pharmacophore hypothesis. *In silico* study through molecular docking simulation method was adopted to analyze the inhibitory activity of the compounds in question. Molecular dynamic simulation (MDs) was performed to assess the stability of the top-ranked phytochemicals. The binding energies of these compounds to the four targets were investigated by the Molecular Mechanics for the Generalized Born Model and Solvent Accessibility method (MM-GBSA). The binding-free energy suggests that cannabinol, cannabichromene, linoelaidic acid and morphinan-6-

one can be utilized as lead compounds in drug discovery and development of AD to inhibit activity of AChE, DCC gene, MAO and HTR2C. The MDs indicated that AChE-Cannabinol, DCC-Cannabicoumaronone, MAO-Linoelaidic acid, and HTR2C-morphinan-6-one were stable over the entire course of 100 ns suggesting their role in the regulation of the diseases in which their respective receptors are implicated.

Keywords: *Cannabis sativa*, Alzheimer's disease, Molecular dynamic simulation, molecular docking, pharmacophore modeling**.**

Introduction

Over the last two-decade, notable changes have taken place concerning policies about Cannabis cultivation, legalization and consumption [1,2]. Cannabis, contains a wide class of compounds from cannabinoids to tannins, flavonoids and fatty acids [3]. The biological activities of Cannabis have well been studied [4,5]. Our previous works on the effects of Cannabis leaf extracts on brain AChE activity, expression of DDC, serotonin receptors, dopamine and numerous endogenous substances established a modulation of functions and activities [3,6,7]. However, there are limited studies focusing on the effects of individual phytochemical isolated from the hemp leaf (Cannabis). This *in-silico* analysis was designed to correlate the binding efficacy of constituents of the Cannabis leaf extracts previously identified through gas chromatography-mass spectrometry (GC-MS) with specific proteins implicated in diverse neurological diseases especially AD [7]. The relationship between small molecules and amyloid proteins have resulted in a huge impact in AD, especially in amyloid folding, metabolism, and brain imaging. Amyloid plaque amelioration or prevention have, until recently, driven drug development, and only a few drugs have advanced in the management of AD [8].

Cognitive decline and a variety of other intellectual impairment symptoms are hallmarks of AD. It is currently one of the most difficult advanced neurodegenerative illnesses to treat [9]. Several theories on the pathophysiology of AD have been proposed throughout the years, including the amyloid cascade, tau protein, and cholinergic hypothesis [10]. The debilitating effects associated with AD such as neuroinflammation, oxidative damage, loss of neurons and synapses have all been found to be altered by several types of small-molecule drugs known as autophagy modulators with

notable results obtained via modulation of the activities of several proteins including AChE, MAO and serotonin [11,12].

Since all recent clinical studies against AD failed to show any efficacy against sporadic or late-onset cases, a greater knowledge of AD mechanisms has enabled new therapeutic or preventive techniques at various phases of the study [13]. Cannabinoids, on the other hand, have pleiotropic effects, which means they target many processes in tandem, such as amyloid beta (Aβ) and tau aberrant processing, neuroinflammation, excitotoxicity, mitochondrial dysfunction, and oxidative stress [14]. Although most of the recent inconclusive AD clinical trials focused on brain amyloidosis and Aβ, with promising pharmacological therapies in phase three clinical trials [15], AD is a multifactorial disease and contemporary studies are focusing on a broader range of symptoms. The cannabinoid system is now considered as a potential target for AD therapeutic intervention, and the limited clinical evidence available also supports that cannabis drugs can improve behavioral symptoms associated with AD, particularly as AChE and MAO inhibitors [15]. A clinical trial on dronabinol, a synthetic analogue of tetrahydrocannabinol, demonstrated a reduced in severity of aberrant behaviors and increased body weight on patients with dementia of the Alzheimer type [16] .

Studies have highlighted specific receptors important for AD therapy [17-20]. Specifically, MAO inhibitors improve cognitive deficits and reverse Aβ pathology by modulating proteolytic cleavage of amyloid precursor protein and reducing Aβ protein fragments [21]. Serotonin receptor was reported to play a crucial role in cognition and its deregulation is associated with AD, depression, and other central nervous system disorders making this receptor a potential target for cognitive disorder [22,23]. Cholinergic deficit is evident in AD making AChE a target of investigation in tissues involved making its inhibitors a pivotal molecule to the field of drug discovery for AD management [24,25]. Equally, DDC is thought to modulate tau in disease. This enzyme is involved in the decarboxylation of L-DOPA in the dopamine and serotonin biosynthetic pathway. DDC was identified as a novel genetic modulator of tauopathy [26]. Thus, inhibitors of these receptors may be considered as promising therapeutic agents for AD.

This study was therefore, designed to investigate the interactions of some cannabinoids, fatty acids, and other compounds derived from cannabis *sativa* leaf extracts with AChE, DDC, MAO-B, and

HTR2C through computational predictions. These targets were selected in the context of contemporary drug discovery for the identification of new AD therapies. In addition, conventional anti-Alzheimer agents, i.e. donepezil, carbidopa, safinamide, and ritanserin were also docked against the respective protein receptors, for suitable comparison with the test compounds.

MATERIALS AND METHODS

Computational study

The complete workflow of the present study is provided in Figure 1.

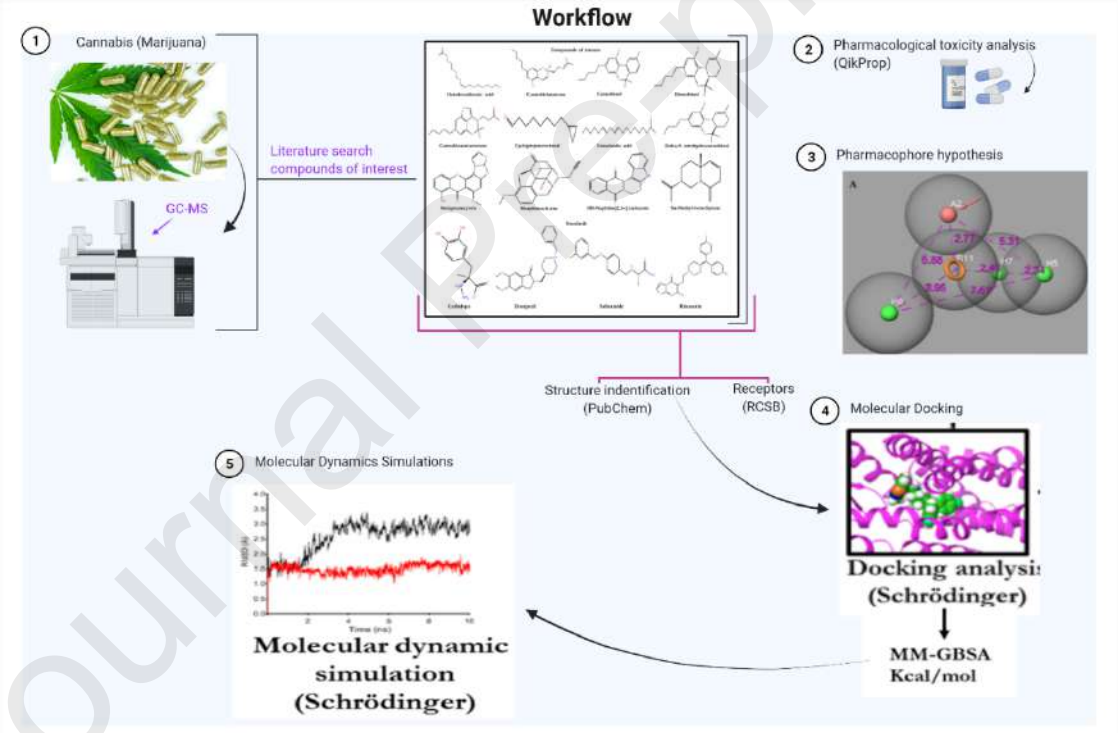

Figure 1: Overview of the study design

Computational pharmacokinetics

Absorption, distribution, metabolism, excretion and toxicity properties (ADMET profiling) of the compounds were performed by toxicity prediction protocol QikProp as previously described [27]. The molecular weight of the ligands (acceptable range: 130.0–725 g/mol), number of permissible

violations of Lipinski's rule of five (acceptable range: maximum is 4) [28], inhibitory concentration (IC_{50}) value for blockage of HERG K^+ channels (concern below −5.0), octanol/water partition coefficient log p (acceptable range: −2.0 to 6.5), skin permeability, log Kp (acceptable range: −8.0 to −1.0), aqueous solubility; S in mol/L (acceptable range: −6.5 to .5) and the brain/blood partition coefficient (acceptable range: −3.0 to 1.2) were all reported [29,30].

Ligand preparation

The two-dimensional (2D) chemical structures of all the isolated compounds were retrieved from the PubChem compound database, which is available at NCBI (http://www.pubchem.ncbi.nlm.nih.gov). Three-dimensional (3D) geometry of the compounds was prepared and generated using the LigPrep module, Schrödinger v2020-3. For docking purposes, low energy ionization and tautomeric states within the pH range of 7.4 ± 0 were generated by Epik [31,32]. During this process, all possible conformations of the ligands were considered. Finally, energy minimization was achieved using the Optimized Potentials for Liquid Simulations (OPLS-2005) force field [33,34].

Target selection and structure preparations

In this study four protein receptors were considered after an extensive literature search; AChE, DDC, MAO B(MAOB) and HTR2C were retrieved from the protein data bank (PDB) at [35], 1JS3 [36], 2V5Z [37], and 6BQH [38]. The protein preparation wizard (PPW) in Maestro v12.8 (Schrödinger) was used to prepare the receptors and the bond orders were corrected. In addition, the crystallographic water molecules were removed, and the hydrogen atoms were added via PROPKA at pH 7.0. The missing side chains atoms and the loops were corrected by Prime, and the het states were generated by Epik as well. The default restrained minimization (RMSD = 0.30 Å) achieved and the OPLS-2005 force field selected for docking [39].

Pharmacophore modelling

The energy-optimized pharmacophore (e-pharmacophore) model combines the advantages of structure-based and ligand-based drug-design theories and can be used to screen small molecules based on pharmacophore properties. Using the Pharmacophore hypothesis module in Schrödinger

suite, pharmacophore sites generated from the receptor-ligand complexes of each receptor, preserving a maximum of seven features as default. The chemical properties include hydrogen-bond acceptor (A), represented as vectors, hydrogen-bond donor (D) as projected points, aromatic ring (R) as ring, positive ionizable (P), and negative ionizable (N). Explicit matching required in the e-pharmacophore approach for generation of the most energetically favorable site. The hypothesis settings were configured to treat atoms as projected points with a radius scaling factor of 0.50 and limit excluded volume shell to 5.0 Å. In addition, common features identified by pharmacophoric points were chosen to satisfy criteria for their positions and directions [40].

Receptor grid generation

The grid boxes for all the receptors were generated using the receptor grid generation module by creating an enclosed box around the centroid of the co-crystalized ligands associated with each of the receptors (the binding pocket). This process ensures that the docked ligands will be confined to the enclosing box by preventing non-specific binding [41]. The scaling factor and partial charge cutoff where 1.0 and 0.25, respectively while for the enclosing box, the centroid of ligand with their respective coordinates were selected. The grid box was defined by selecting the co-crystallized ligands (donepezil, carbidopa, safinamide, and Ritanserin of 4EY7, 1JS3, 2V5Z, and 6BQH, respectively) to keep the center of each docked ligand with same dimensions of binding box. The receptors coordinates(xyz) for docking were set as follow 4EY7 (x = -13.96, y = -44.02, z = 27.93), 1JS3 (x = 43.25, y = 36.78, z = 67.07, 2V5Z (x = 51.09, y = 156.47, z = 28.56), and 6BQH (x = 38.09, y = 31.07, z = 56.76).

Molecular docking

The docking studies with Glide has extensively been used for various protein-ligand docking calculations and the results were incredibly insightful when an extra precision (XP) scoring function of Glide incorporated [42,43]. In this study, the prepared and minimized compounds were docked into the active sites of the selected receptors using the Glide-XP (Extra-Precision-algorithm) docking method and the interactions of the ligands with receptors deciphered [44,45]. The Glide-XP takes into an account the receptor as rigid and the ligand sampling flexible. The OPLS-2005 force field was used for docking calculations [39]. In addition, a self-docking approach

employed to validate the docking results. The co-crystal ligands were redocked in their respective receptors and the non-covalent interactions such as hydrogen bonding and pi-pi interactions were considered as a standard before proceeding to molecular dynamic simulations. The 2D and the 3D interactions of the complexes were analyzed by ligand interaction diagram and the XP visualizer modules within the Schrödinger suite.

Binding Free Energy calculations

The MM-GBSA approach was used for binding affinity delta (ΔG) prediction, to better understand the binding of ligands with the selected receptors [46]. The more negative energy in terms of delta (ΔG) depicts the better binding of the ligands towards its receptors. The delta (ΔG) calculated via the formula:

$$\Delta G_{Bind} = G_{Complex} - G_{Recpetor} - G_{Ligand}$$

All the complexes were subjected to MM-GBSA algorithm, and their binding free energy was calculated [44,47].

Molecular dynamics simulation

The MD simulations were performed using the Desmond package and the simulation systems for the complexes were prepared in a similar manner to our previously published method [48]. The system builder module was used, and the ligand-protein complexes were first solvated with transferable intermolecular potential with 3 points (TIP3P) water model, extending 10 Å beyond any of the complex's atoms in orthorhombic box shape (buffered distance). The full system neutralized by adding the counter ions (Na^+, and Cl^- ions). The system was set to 0.15 M sodium and chloride ions to mimic physiological condition. The relaxation protocol was performed under NPT ensemble using the thermostat method Nose-Hoover chain and Martyna-Tobias-Klein barostat methods applying a constant temperature of 300ºK and 1.01325 bar of pressure, respectively, with isotropic coupling style. The short-range coulombic interactions were analyzed

using a cut-off radius of 9.0 Å and the short-range method. The smooth particle mesh ewald method was used for handling long-range coulombic interactions and reversible reference system propagator algorithm (RESPA)-based constraints allowing 2 fs time steps. The MD simulation was carried out for 100 ns and the trajectory sampling was set at an interval of 100 ps with 1000 frame numbers. Simulations were run with the OPLS-2005 force field. The trajectories were analyzed by simulation interaction diagram and the GraphPad Prism v5.0.0 was used to plot the data.

Results

Chemical structures of ligands

The 2D structures of the twelve test compounds, namely 8a-Methyl-5methylene, cyclopropaneoctanal, octadecadienoic acid, linoelaidic acid, cannabichromene, 5H-naphtho[2,3c]carbazole, cannabicoumaronone, Morphinan-6-one, Dronabinol, delta-9-tetrahydrocannabinol, cannabinol and sterigmatocystin (Figure 2) were modeled and used as a ligands for docking studies against four target proteins (AChE, DCC, MAO-B and HTR2C) (Figure 3).

Toxicological properties of the ligands

To get more insights on the pharmacological properties of the ligands, ADMET and drug -likeness properties of the Cannabis ligands against the target proteins were analyzed via QikProp. The ADMET properties of the 8a-Methyl-5methylene, cyclopropaneoctanal, octadecadienoic acid, linoelaidic acid, cannabichromene, 5H-naphtho[2,3c]carbazole, cannabicoumaronone, morphinan-6-one, dronabinol, delta-9-tetrahydrocannabinol, cannabinol and sterigmatocystin were evaluated and displayed in Table 1. The selected properties such as the molecular weight (MW), Lipinski's Rule of five (RO5), Q plog HERG, Q plog Po/W (octanol/water partition coefficient), Q plog KP (skin permeability), Q plog S (aqueous solubility) and Q plog BB (brain/blood partition coefficient) were all calculated. The molecular weight (<500), as well as the Lipinski RO5 for all the compounds, were analyzed in the acceptable range. The partition coefficient (QPlogPo/w), a very important parameter ranges for all the compounds from -2.102 to

6.037 and the solubility of water (QPlogS) from -6.59 to -2.28 with an exception for Cannabichromene (-6.99) and cannabinol (-6.75). The human Ether-a-go-go-Related Gene (hERG) K+ channels from -5.46 to -3.57 IC_{50} which were values responsible for the blockage. Table 1 revealed each of these values and they were all under the acceptable range, which signifies the druggability of the cannabis compounds.

Pharmacophore modeling

Pharmacophore model is in part an important concept in medicinal chemistry. It is defined as the spatial orientation of diverse features of a molecule required for the activity towards a biomolecular target. The pharmacophore hypothesis is a ligand-based method which can be employed for virtual screening purposes. Briefly, the ligand-based virtual screening module of Schrödinger was used to develop this hypothesis and multiple ligands were used to create the model. In addition, others such as 25% match, a range of 4-7 number of features and 5 selected as the preferred minimum number of features. Finally, the pharmacophore hypo scoring function was used and the highest-scoring function of 0.82, 7 active ligands (PubChem ID: 2543, 6453891, 16078, 30219, 625303, 5280389, and 5492746) have the features AHHHR with ROC of 0.53 and area under accumulating curve of 0.73 as shown in Figure 4. The pharmacophore modeling of the compounds and the standards are shown in Figure 5.

Molecular docking

The docking score results of the ligands against the four selected targets of AD are presented in Table S2-S5. The docking scores of the compounds were between −5.60 and −11.20 kcal/mol. Morphinan-6-one achieved the highest docking score of −11.20 kcal/mol, closely followed by dronabinol and 5H-naphtho[2,3c]carbazole with docking scores of −9.10 kcal/mol and −8.90 kcal/mol for AChE, morphinan-6-one with a docking score of −7.60 kcal/mol, cannabichromene, cannabicoumaronone and dronabinol with scores of −5.20 kcal/mol, -4.8 kcal/mol and -4.8 kcal/mol for DCC, delta-9-tetrahydrocannabinol with a docking score of -10.0 kcal/mol, cannabichromene and cannabicoumaronone with docking score of -9.90 kcal/mol and -9.80 kcal/mol for MAO-B and Cannabinol with a score of −9.10 kcal/mol, followed by

cannabichromene and cannabicoumaronone with scores of −8.40 kcal/mol and −8.20 kcal/mol for HTR2C, respectively.

The molecular interactions of the amino acid residues of AChE, DCC, MAO-B and HTR2C with the standards (donepezil, carbidopa safinamide and ritanserin), 8a-Methyl-5methylene, cyclopropaneoctanal, octadecadienoic acid, linoelaidic acid, cannabichromene, 5H-naphtho[2,3c]carbazole, cannabicoumaronone, morphinan-6-one, dronabinol, delta-9-tetrahydrocannabinol, cannabinol and sterigmatocystin were determined and the results are displayed in Figures 6-10. The molecular bonding of the amino acid residues of AChE with the standard (donepezil), and the compounds are depicted in Figures 6 and 7 and Table S1 and S2. The molecular bonding of the amino residues of dopa decarboxylase (DCC) gene with the standard (carbidopa) and the compounds were reported in Figures 8 and Table S1 and S3. The molecular interactions of the amino residues of MAO-B with the standard (safinamide), and the compounds are represented in Figures 9 and Table S1 and S4. The molecular interactions of the amino residues of HTR2C with the standard (ritanserin), and the compounds are represented in Figures 10 and Table S1 and S5.

MM-GBSA analysis

The results are presented in Table S1-S5. The collective approach of molecular docking and free energy results in a good performance to predict the binding-free energy indicating that cannabinol, cannabichromene, linoelaidic acid and morphinan-6-one may be utilized to steer discovery and optimization of AChE, DCC gene, MAO-B and HTR2C. As shown in the Table S1-S5, out of twelve candidate compounds, cannabinol exhibited best binding energy (ΔG_{Bind}= -58.73 kcal/mol) compared to least binding compound octadecadienoic acid, with affinity of (ΔG_{Bind} = -20.27 kcal/mol) for AChE, cannabichromene revealed best binding energy (ΔG_{Bind} = -61.40 kcal/mol) compared to least binding compound 5H-naphtho[2,3c]carbazole (ΔG_{Bind} = -31.44 kcal/mol) for DCC gene, linoelaidic acid showed best binding compound (ΔG_{Bind} = -89.38 kcal/mol) compared to least compound 8a-methyl-5-methylene-3-(prop-1-en-2-yl)- (ΔGTotal = -6.92 kcal/mol) for MAO, and morphinan-6-one revealed best binding affinity of (ΔG_{Bind} = -73.10

kcal/mol) compared to least compound 8a-methyl-5methylene-3-(prop-1en-2-yl)- (ΔG_{Bind} = -39.04 kcal/mol) for HTR2C receptor. In contrast, the standard compounds free binding affinity revealed that donepezil and ritanserin (ΔG_{Bind} = -81.35 and 115.81 kcal/mol) have better binding affinity than the compounds with the exception been safinamide and carbidopa with less binding affinity compared to the compounds (ΔG_{Bind} = -76.41 and -25.78 kcal/mol).

Molecular dynamic simulation analysis

The binding interaction between proteins and small molecules has been implicated in various biological processes with clinical implications. Therefore, it is idea to investigate the binding phenomenon based on the stability and flexibility of the ligands and the receptors under study. The top ligands based on their binding energy and non-covalent bonding interactions such as hydrogen bonding and pi-pi interactions from the molecular docking calculations were subjected to MDs (molecular dynamics) and their dynamics validated against the co-crystal compounds at 100ns each. A similar MD protocol in our previous studies was applied in this work [49]. The structural parameters such as the root mean square fluctuation (RMSF), root mean square deviation (RMSD), and the ligand properties including the radius of gyration (Rgyr) were deciphered throughout the 100 ns simulation time. In this study, the four complexes retrieved from docking based on better interactions such as H-bonding networks and pi-pi interactions and importantly more favorable binding free energy in terms of ΔG with the active site residues were deciphered and further validated including and or comparison with the co-crystal ligands in Figure 11-14 and simulation properties in Table 2.

The complex structures of AChE-Donepezil and AChE-Cannabinol (Figure 11 A and B, respectively), DCC-carbidopa and DCC-Cannabicoumaronone (Figure 12 A and B, respectively), MAO-B-safinamide and MAO-B-Linoelaidic acid (Figure 13 A and B, respectively), and HTR2C-Ritanserin and HTR2C-morphinan-6one (Figure 14 A and B, respectively) were set up to mimic the biological behavior by the addition of water, Na^+ and Cl^- as presented in Figures 11-14 C and D for receptor complexed with standard drugs and receptor-ligand complexes, respectively. Based on the post-MDs analysis, the RMSD and RMSF of the analyzed complexes were depicted in Figures 11-14 E and F, respectively. The ligand properties for the isolated compounds and their respective standard drugs were also evaluated to include ligand RMSD and rGyr (Figure 11-14 G).

The RMSD of all the complexes was analyzed to include the Cα, protein and ligand. The result is a graphical output showing the RMSD values on the Y axis against the simulation time (ns) on the X-axis. The RMSD of the complexes of AChE-Donepezil and AChE-Cannabinol were found to attain stability at about 400 ns and this stability was maintained throughout the simulation (Figure 11E). The RMSD of the Cα of Donepezil and Cannabinol were stable from the beginning and throughout the simulation course. The RMSD of the Cα, protein, and the ligand of carbidopa was stable throughout the simulation period. The RMSD of the protein atoms involved in binding Cannabicoumaronone showed some degree of fluctuation from the beginning to around 200 ns, stability was attained after this time to about 600 ns and then towards the 100 ns simulation time. Other properties of the RMSD were stable throughout (Figure 12). For MAO-B, stability of the RMSD of all the properties of both the standard drugs and Linoelaidic acid were attained at 200 ns with a similar low RMSF value for Safinamide and Linoelaidic acid. The properties of the ligands also showed relative stability throughout the simulation time (Figure 13). The complexes of HTR2C-Ritanserin and HTR2C-morphinan-6one in terms of the observed RMSD and the ligand properties were stable from the beginning to the end of the 100 ns simulation time. The RMSF of the two complexes was also similar with a relatively low fluctuation (Figure 14).

Discussion

Drug-likeness is defined as a model of several molecular properties and structural features which validate whether a particular compound can be a potential drug. *In-vivo* evaluation of drug-like properties of any compound is very costly and time-consuming while the *in-silico* approaches are very cost-effective and rapid. The recorded findings showed that all the compounds that were studied followed Lipinski's RO5. Furthermore, the profiles of ADMET were measured and it shows a lesser value which is a marker of better druggability when using the Qikprop analysis. Partition coefficient (QPlogPo/w) values are correlated with absorption potential as well as the distribution rate of the drugs within the body. The ADMET analysis revealed that all the compounds lies in the acceptable range of druggability, making them possible potential drug-like molecules that could switch off the proteins involved in AD.

The 3D pharmacophore model was developed using a five-point hypothesis AHHHR, which consists of three hydrophobic (H), and two aromatic rings (R). This hypothesis (AHHHR)

was selected based on the highest-scoring function. Besides, to validate the model, 25% match, a range of 4-7 number of features and 5 was selected as the preferred minimum number of features. For the AHHHR hypothesis, another reliable metric to evaluate the performance of the pharmacophore model is the AUC of the ROC. The AUC values revealed 0.73. Stranded criteria $0.50 \leq AUC < 0.7$ is poor; and $AUC < 0.5$ is a failure [50]. Calculated AUC ranging from the model were excellent and model achieved good value of 0.73 AUC and 0.53 ROC. The comparative alignment of the developed pharmacophore model with that of AChE, DDC gene, MAO-B and HTR 2C and the vital interactions of the AHHHR model and may be employed for validating the developed model [51]. As a result of the pharmacophore model to the docked complex of this series AAHPRR.15, it was observed from the results that the ligands achieved the same property. The AAHPRR. 15 model shown, explains a long-range between each of the features. The features of the catalytic pocket R11 and A2 are fully stressed. Initially, A2 features revealed pi-cation interactions with Tyr337 and Trp86. R11 bind with amino acid residue Trp86 in internal catalytic site and H5 in peripheral site did not interact with any residues. The A2 and H9 revealed vital interactions for peripheral site binding via the pi-pi interaction of AChE inhibitors with Trp286 and displayed the H-bond with Phe296.

Molecular docking is a reliable practical instrument employed in computational analysis for drug development essential in determining the binding energy of a ligand with a receptor [41]. The docking scores of the studied ligands showed that Morphiana-6-one is a better modulator of AChE compared to others. The fatty acid compound 9, 12-Octadecadienoic acid (Z, Z) had the least binding affinity with AChE. Also, the docking score of these compounds with DDC revealed a similar trend with Morphinan-6-one. Cannabichromene, sterigmatocystin and dronabinol were next in ranking. However, cyclopropaneoctanal had the least binding affinity.

Furthermore, docking of ligands with MAO-B and HTR2C showed that the cannabinoids had the best interactions. For MAO-B, the most psychoactive cannabinoid, tetrahydrocannabinol ranked highest, closely followed by cannabichromene, cannabicoumaronone and dronabinol. Cannabinol, cannabichromene and cannabicoumaronone exhibited the best scores for HTR2C. In general, the high docking score exhibited by these compounds may denote their modulatory activities with the proteins [52]. This study also showed that the compounds interacted with several amino acid residues including ARG A: 296, PHE A:295, SER A:125, and TYR A:124; majorly through

several forces such as conventional hydrogen bonding and pi-pi (π-π) stacking. For AChE and DDC, although most ligands had one form of interaction or the other, Morphinan-6-one was the most active as it interacted with the highest number of amino acid residues. This also corroborates the high docking score recorded for this ligand and the receptors, therefore, suggests that it can serve as a potential acetylcholinesterase and dopamine decarboxylase inhibitor. Cannabicoumaronone interacted with the highest number of amino acid residues of MAO-B, while Sterigmatocystin and 5H-naphtho[2,3c]carbazole were the most active compounds against HTR2C when compared with the other compounds. The molecular docking approach conducted in this study was to determine the most favorable position of a ligand molecule inside the binding pocket of a receptor.

The MM-GBSA was critically investigated to compute all the free energies that were binding which means; the binding of ΔG indicates the affirmation of the outcome when it comes to solvation, VDW, and hydrophobic, VDW components. The Prime MM-GBSA was computed, combined with compounds (AChE, DCC gene, MAO-B and HTR2C). The stability of the receptor-ligand complex is considered strong when the computed values of binding free energies are more negative [53] The obtained binding free energies of all reported compounds with AChE, DCC gene, MAO-B and HTR2C have the binding free energies less than the standard compounds except carbidopa and ritanserin. The obtained free energies of the compounds against MAO-B and HTR2C have binding affinity less than -40.00 kcal/mol. In the case of 8a-Methyl-5-methylene-3-(prop-1-en-2-yl)-, the resulting binding free energy is -6.92 and -39.04 kcal/mol, respectively and indicating the probability of it forming a slightly weaker complex with MAO-B and HTR2C more than the other compounds. Therefore, Cannabis phytochemicals displayed promising Prime MM-GBSA bonding with the free energies after binding with AChE, DCC gene, MAO-B and HTR2C, indicating that documented phytochemicals bring about a firm and hard forms of binding with the AChE, DCC gene, MAO-B and HTR2C and these complexes are thermodynamically favorable.

MDs is a computational method employed to mimic the dynamic behavior of molecular systems concerning time, treating all the entities in the simulation box as flexible [54]. This method was adopted to infer the motions and flexibility of the protein, which contributes to the interaction dynamics of the complexes. Analysis of RMSD is very crucial in MDs trajectory and depicts the difference between the backbone of a given receptor from its initial structural conformation to its

final. The stability of AChE, DCC gene, MAO-B and HTR2C relative to their conformation validated against their reference native conformation by the deviation observed during the 100 ns. The RMSD of the residues, ligands and Cα atoms were analyzed as well. The analysis of simulations of all the receptors under study showed minor deviations and indicating the stable complexes with better binding towards its receptors suggesting possible potential drug molecules [55].

RMSF indicated the fluctuation of the receptor residues involved in binding in the binding pocket of the AChE, DCC gene, MAO-B and HTR2C from the MDs trajectory. The RMSF analysis revealed minor fluctuations between the positions of atoms to their reference during the entire 100 ns. Rigid protein structures usually have low fluctuation while bends and coils proteins usually have higher values because of the free movement of atoms. The rGyr shows the compactness of folded protein. The rGyr values observed in this study were between the range of 3-7 Å. The rGyr of a globular folded state of a protein should be low and protein with more numbers of loops and turns and in an expanded state should be fairly high [55].

Conclusion

In the present study, the computational tools and techniques of docking, pharmacophore modelling, pharmacokinetics and molecular dynamics were employed to have insight into the therapeutic properties and dynamics of *Cannabis sativa* compounds. In combination with physics based binding free energy calculations (MM-GBSA), we revealed the compounds cannabinol, cannabichromene, linoelaidic acid and morphinan-6-one as potential drug like molecules which can be utilized to lead drug discovery and AD therapy by inhibiting actions of AD target proteins such as AChE, DCC, MAO-B, and HTR2C. Studies are warranted to validate the actions of these ligands *in vitro*, and also to investigate their mechanism of action following binding to the receptors.

Acknowledgment

Authors would like to acknowledge the National Integrated Cyberinfrastructure system, Center for High Performance Computing (CHPC), Department of Science and Technology, Republic of South Africa for the license to the Lengau cluster and other modules under the Schrödinger suite.

References

1. Whiting, P.F.; Wolff, R.F.; Deshpande, S.; Di Nisio, M.; Duffy, S.; Hernandez, A.V.; Keurentjes, J.C.; Lang, S.; Misso, K.; Ryder, S. Cannabinoids for medical use: a systematic review and meta-analysis. *Jama* **2015**, *313*, 2456-2473.
2. Hall, W. *Health and Social Effects of Nonmedical Cannabis Use (The)*; World Health Organization: 2016.
3. Taiwo, O.A.; Dosumu, O.A.; Ugbaja, R.N.; Rotimi, S.O.; Owolabi, O.P.; Ojo, O.A. Oral administration of marijuana produces alterations in serotonin 5-hydroxytryptamine receptor 3A gene (HTR3A) and electrolyte imbalances in brain of male Wistar rats. *Molecular biology research communications* **2021**, *10*, 5.
4. Moreno-Sanz, G.; Ferreiro Vera, C.; Sánchez-Carnerero, C.; Nadal Roura, X.; Sánchez de Medina Baena, V. Biological Activity of Cannabis sativa L. Extracts Critically Depends on Solvent Polarity and Decarboxylation. *Separations* **2020**, *7*, 56.
5. Rožanc, J.; Kotnik, P.; Milojević, M.; Gradišnik, L.; Knez Hrnčič, M.; Knez, Ž.; Maver, U. Different Cannabis sativa Extraction Methods Result in Different Biological Activities against a Colon Cancer Cell Line and Healthy Colon Cells. *Plants (Basel)* **2021**, *10*, doi:10.3390/plants10030566.
6. Taiwo, O.A.D.O.A.; Akinloye, O.A.; Oni, E.O.; Owolabi, O.P.; Ojo, O.A. TIME-COURSE EFFECTS OF Cannabis sativa ON BRAIN ACETYLCHOLINESTERASE (AChE) ACTIVITY AND EXPRESSION OF DOPA DECARBOXYLASE GENE (DDC). **2020**.
7. Dosumu, O.A.; Owolabi, O.P.; Ugbaja, R.N.; Popoola, A.; Rotimi, S.O.; Taiwo, O.A.; Ojo, O.A. Administration of Cannabis causes alterations in monoamine oxidase B and serotonin receptor 2C gene expressions in Wistar rats. *Acta facultatis medicae Naissensis* **2021**, *38*, 35-46.
8. Patel, V.; Zhang, X.; Tautiva, N.A.; Nyabera, A.N.; Owa, O.O.; Baidya, M.; Sung, H.C.; Taunk, P.S.; Abdollahi, S.; Charles, S.; et al. Small molecules and Alzheimer's disease: misfolding, metabolism and imaging. *Curr Alzheimer Res* **2015**, *12*, 445-461, doi:10.2174/1567205012666150504145646.
9. Fargo, K.; Bleiler, L. Alzheimer's association report: 2014 Alzheimers disease facts and figures. *Alzheimers Dement* **2014**, *10*, e47-e92.
10. Ojo, O.A.; Adegboyega, A.E.; Johnson, G.I.; Umedum, N.L.; Onuh, K.; Adeduro, M.N.; Nwobodo, V.O.; Elekan, A.O.; Alemika, T.E.; Johnson, T.O. Deciphering the interactions of compounds from Allium sativum targeted towards identification of novel PTP 1B inhibitors in diabetes treatment: A computational approach. *Informatics in Medicine Unlocked* **2021**, *26*, 100719.
11. Deng, Z.; Dong, Y.; Zhou, X.; Lu, J.-H.; Yue, Z. Pharmacological modulation of autophagy for Alzheimer's disease therapy: Opportunities and obstacles. *Acta Pharmaceutica Sinica B* **2021**.
12. Oliver, D.M.; Reddy, P.H. Small molecules as therapeutic drugs for Alzheimer's disease. *Molecular and Cellular Neuroscience* **2019**, *96*, 47-62.
13. Thomas, M.H.; Olivier, J.L. Arachidonic acid in Alzheimer's disease. *Journal of Neurology & Neuromedicine* **2016**, *1*.
14. Damazio, L.S.; Silveira, F.R.; Canever, L.; CASTRO, A.A.; Estrela, J.M.; Budni, J.; Zugno, A.I. The preventive effects of ascorbic acid supplementation on locomotor and acetylcholinesterase activity in an animal model of schizophrenia induced by ketamine. *Anais da Academia Brasileira de Ciências* **2017**, *89*, 1133-1141.

15. Lalli, G.; Schott, J.M.; Hardy, J.; De Strooper, B. Aducanumab: a new phase in therapeutic development for Alzheimer's disease? *EMBO Molecular Medicine* **2021**, *13*, e14781.
16. Volicer, L.; Stelly, M.; Morris, J.; McLAUGHLIN, J.; Volicer, B.J. Effects of dronabinol on anorexia and disturbed behavior in patients with Alzheimer's disease. *International journal of geriatric psychiatry* **1997**, *12*, 913-919.
17. Danysz, W.; Parsons, C.G. Alzheimer's disease, β-amyloid, glutamate, NMDA receptors and memantine--searching for the connections. *British journal of pharmacology* **2012**, *167*, 324-352, doi:10.1111/j.1476-5381.2012.02057.x.
18. Stanciu, G.D.; Luca, A.; Rusu, R.N.; Bild, V.; Beschea Chiriac, S.I.; Solcan, C.; Bild, W.; Ababei, D.C. Alzheimer's Disease Pharmacotherapy in Relation to Cholinergic System Involvement. *Biomolecules* **2019**, *10*, 40, doi:10.3390/biom10010040.
19. Moutinho, M.; Landreth, G.E. Therapeutic potential of nuclear receptor agonists in Alzheimer's disease. *Journal of Lipid Research* **2017**, *58*, 1937-1949, doi:https://doi.org/10.1194/jlr.R075556.
20. Saeedi, M.; Rashidy-Pour, A. Association between chronic stress and Alzheimer's disease: Therapeutic effects of Saffron. *Biomedicine & Pharmacotherapy* **2021**, *133*, 110995, doi:https://doi.org/10.1016/j.biopha.2020.110995.
21. Cai, Z. Monoamine oxidase inhibitors: promising therapeutic agents for Alzheimer's disease (Review). *Mol Med Rep* **2014**, *9*, 1533-1541, doi:10.3892/mmr.2014.2040.
22. Hu, L.; Wang, B.; Zhang, Y. Serotonin 5-HT6 receptors affect cognition in a mouse model of Alzheimer's disease by regulating cilia function. *Alzheimer's research & therapy* **2017**, *9*, 1-17.
23. Ferris, C.F.; Kulkarni, P.; Yee, J.R.; Nedelman, M.; de Jong, I.E.M. The Serotonin Receptor 6 Antagonist Idalopirdine and Acetylcholinesterase Inhibitor Donepezil Have Synergistic Effects on Brain Activity—A Functional MRI Study in the Awake Rat. *Frontiers in Pharmacology* **2017**, *8*, doi:10.3389/fphar.2017.00279.
24. Talesa, V.N. Acetylcholinesterase in Alzheimer's disease. *Mech Ageing Dev* **2001**, *122*, 1961-1969, doi:10.1016/s0047-6374(01)00309-8.
25. Rees, T.M.; Brimijoin, S. The role of acetylcholinesterase in the pathogenesis of Alzheimer's disease. *Drugs Today (Barc)* **2003**, *39*, 75-83, doi:10.1358/dot.2003.39.1.740206.
26. Kow, R.L.; Sikkema, C.; Wheeler, J.M.; Wilkinson, C.W.; Kraemer, B.C. DOPA decarboxylase modulates tau toxicity. *Biological psychiatry* **2018**, *83*, 438-446.
27. Ioakimidis, L.; Thoukydidis, L.; Mirza, A.; Naeem, S.; Reynisson, J. Benchmarking the reliability of QikProp. Correlation between experimental and predicted values. *QSAR & Combinatorial Science* **2008**, *27*, 445-456.
28. Lipinski, C.A. Lead- and drug-like compounds: the rule-of-five revolution. *Drug Discovery Today: Technologies* **2004**, *1*, 337-341, doi:https://doi.org/10.1016/j.ddtec.2004.11.007.
29. Guan, L.; Yang, H.; Cai, Y.; Sun, L.; Di, P.; Li, W.; Liu, G.; Tang, Y. ADMET-score–a comprehensive scoring function for evaluation of chemical drug-likeness. *Medchemcomm* **2019**, *10*, 148-157.
30. Ojo, O.A. Exploring the potentials of selected bioactive compounds isolated from Piper guineense Schumach. & Thonn. leaf toward identification of novel pfDHFR and pfDHODH inhibitors as antimalaria agents. *Journal of Applied Pharmaceutical Science* **2021**, *11*, 153-158.
31. Shelley, J.C.; Cholleti, A.; Frye, L.L.; Greenwood, J.R.; Timlin, M.R.; Uchimaya, M. Epik: a software program for pK a prediction and protonation state generation for drug-like molecules. *Journal of computer-aided molecular design* **2007**, *21*, 681-691.
32. Greenwood, J.R.; Calkins, D.; Sullivan, A.P.; Shelley, J.C. Towards the comprehensive, rapid, and accurate prediction of the favorable tautomeric states of drug-like molecules in aqueous solution. *Journal of computer-aided molecular design* **2010**, *24*, 591-604.
33. Fadaka, A.O.; Klein, A.; Pretorius, A. In silico identification of microRNAs as candidate colorectal cancer biomarkers. *Tumor Biology* **2019**, *41*, 1010428319883721.

34. Johnson, T.; Adegboyega, A.; Ojo, O.; Jega, A.; Iwaloye, O.; Ugwah-Oguejiofor, C.; Asomadu, R.; Chukwuma, I.; Ejembi, S.E.; Ugwuja, E. Identification of possible inhibitors of SARS-CoV-2 main protease from some bioactive compounds of Artemisia Annua: An in silico approach. **2021**.
35. Cheung, J.; Gary, E.N.; Shiomi, K.; Rosenberry, T.L. Structures of human acetylcholinesterase bound to dihydrotanshinone I and territrem B show peripheral site flexibility. *ACS medicinal chemistry letters* **2013**, *4*, 1091-1096.
36. Burkhard, P.; Dominici, P.; Borri-Voltattorni, C.; Jansonius, J.N.; Malashkevich, V.N. Structural insight into Parkinson's disease treatment from drug-inhibited DOPA decarboxylase. *Nature structural biology* **2001**, *8*, 963-967.
37. Binda, C.; Wang, J.; Pisani, L.; Caccia, C.; Carotti, A.; Salvati, P.; Edmondson, D.E.; Mattevi, A. Structures of human monoamine oxidase B complexes with selective noncovalent inhibitors: safinamide and coumarin analogs. *Journal of medicinal chemistry* **2007**, *50*, 5848-5852.
38. Peng, Y.; McCorvy, J.D.; Harpsøe, K.; Lansu, K.; Yuan, S.; Popov, P.; Qu, L.; Pu, M.; Che, T.; Nikolajsen, L.F. 5-HT2C receptor structures reveal the structural basis of GPCR polypharmacology. *Cell* **2018**, *172*, 719-730. e714.
39. Shivakumar, D.; Williams, J.; Wu, Y.; Damm, W.; Shelley, J.; Sherman, W. Prediction of Absolute Solvation Free Energies using Molecular Dynamics Free Energy Perturbation and the OPLS Force Field. *Journal of Chemical Theory and Computation* **2010**, *6*, 1509-1519, doi:10.1021/ct900587b.
40. Salam, N.K.; Nuti, R.; Sherman, W. Novel method for generating structure-based pharmacophores using energetic analysis. *Journal of chemical information and modeling* **2009**, *49*, 2356-2368.
41. Fadaka, A.O.; Sibuyi, N.R.S.; Martin, D.R.; Klein, A.; Madiehe, A.; Meyer, M. Development of Effective Therapeutic Molecule from Natural Sources against Coronavirus Protease. *International journal of molecular sciences* **2021**, *22*, 9431.
42. Friesner, R.A.; Murphy, R.B.; Repasky, M.P.; Frye, L.L.; Greenwood, J.R.; Halgren, T.A.; Sanschagrin, P.C.; Mainz, D.T. Extra Precision Glide: Docking and Scoring Incorporating a Model of Hydrophobic Enclosure for Protein−Ligand Complexes. *Journal of Medicinal Chemistry* **2006**, *49*, 6177-6196, doi:10.1021/jm051256o.
43. Ojo, O.A.; Aruleba, R.T.; Adekiya, T.A.; Sibuyi, N.R.S.; Ojo, A.B.; Ajiboye, B.O.; Oyinloye, B.E.; Adeola, H.A.; Fadaka, A.O. Deciphering the interaction of puerarin with cancer macromolecules: An in silico investigation. *Journal of Biomolecular Structure and Dynamics* **2020**, 1-12.
44. Musumeci, D.; Ullah, S.; Ikram, A.; Roviello, G.N. Novel insights on nucleopeptide binding: A spectroscopic and in silico investigation on the interaction of a thymine-bearing tetrapeptide with a homoadenine DNA. *Journal of Molecular Liquids* **2022**, *347*, 117975, doi:https://doi.org/10.1016/j.molliq.2021.117975.
45. Friesner, R.A.; Banks, J.L.; Murphy, R.B.; Halgren, T.A.; Klicic, J.J.; Mainz, D.T.; Repasky, M.P.; Knoll, E.H.; Shelley, M.; Perry, J.K.; et al. Glide: A New Approach for Rapid, Accurate Docking and Scoring. 1. Method and Assessment of Docking Accuracy. *Journal of Medicinal Chemistry* **2004**, *47*, 1739-1749, doi:10.1021/jm0306430.
46. Mulakala, C.; Viswanadhan, V.N. Could MM-GBSA be accurate enough for calculation of absolute protein/ligand binding free energies? *Journal of Molecular Graphics and Modelling* **2013**, *46*, 41-51, doi:https://doi.org/10.1016/j.jmgm.2013.09.005.
47. Yu, Z.; Jacobson, M.P.; Friesner, R.A. What role do surfaces play in GB models? A new-generation of surface-generalized born model based on a novel gaussian surface for biomolecules. *Journal of computational chemistry* **2006**, *27*, 72-89.
48. Adekiya, T.A.; Aruleba, R.T.; Klein, A.; Fadaka, A.O. In silico inhibition of SGTP4 as a therapeutic target for the treatment of schistosomiasis. *Journal of Biomolecular Structure and Dynamics* **2020**, 1-9.

49. Fadaka, A.O.; Aruleba, R.T.; Sibuyi, N.R.S.; Klein, A.; Madiehe, A.M.; Meyer, M. Inhibitory potential of repurposed drugs against the SARS-CoV-2 main protease: a computational-aided approach. *Journal of Biomolecular Structure and Dynamics* **2020**, 1-13.
50. Hanley, J.A.; McNeil, B.J. The meaning and use of the area under a receiver operating characteristic (ROC) curve. *Radiology* **1982**, *143*, 29-36, doi:10.1148/radiology.143.1.7063747.
51. Roberts, B.C.; Mancera, R.L. Ligand− protein docking with water molecules. *Journal of chemical information and modeling* **2008**, *48*, 397-408.
52. Ojo, O.A.; Ojo, A.B.; Okolie, C.; Nwakama, M.-A.C.; Iyobhebhe, M.; Evbuomwan, I.O.; Nwonuma, C.O.; Maimako, R.F.; Adegboyega, A.E.; Taiwo, O.A. Deciphering the interactions of bioactive compounds in selected traditional medicinal plants against Alzheimer's diseases via pharmacophore modeling, auto-QSAR, and molecular docking approaches. *Molecules* **2021**, *26*, 1996.
53. Lokhande, K.B.; Ballav, S.; Yadav, R.S.; Swamy, K.V.; Basu, S. Probing intermolecular interactions and binding stability of kaempferol, quercetin and resveratrol derivatives with PPAR-γ: docking, molecular dynamics and MM/GBSA approach to reveal potent PPAR-γ agonist against cancer. *Journal of Biomolecular Structure and Dynamics* **2020**, 1-11.
54. Salmaso, V. Exploring protein flexibility during docking to investigate ligand-target recognition. **2018**.
55. Shukla, R.; Tripathi, T. Molecular Dynamics Simulation of Protein and Protein–Ligand Complexes. In *Computer-Aided Drug Design*; Springer: 2020; pp. 133-161.

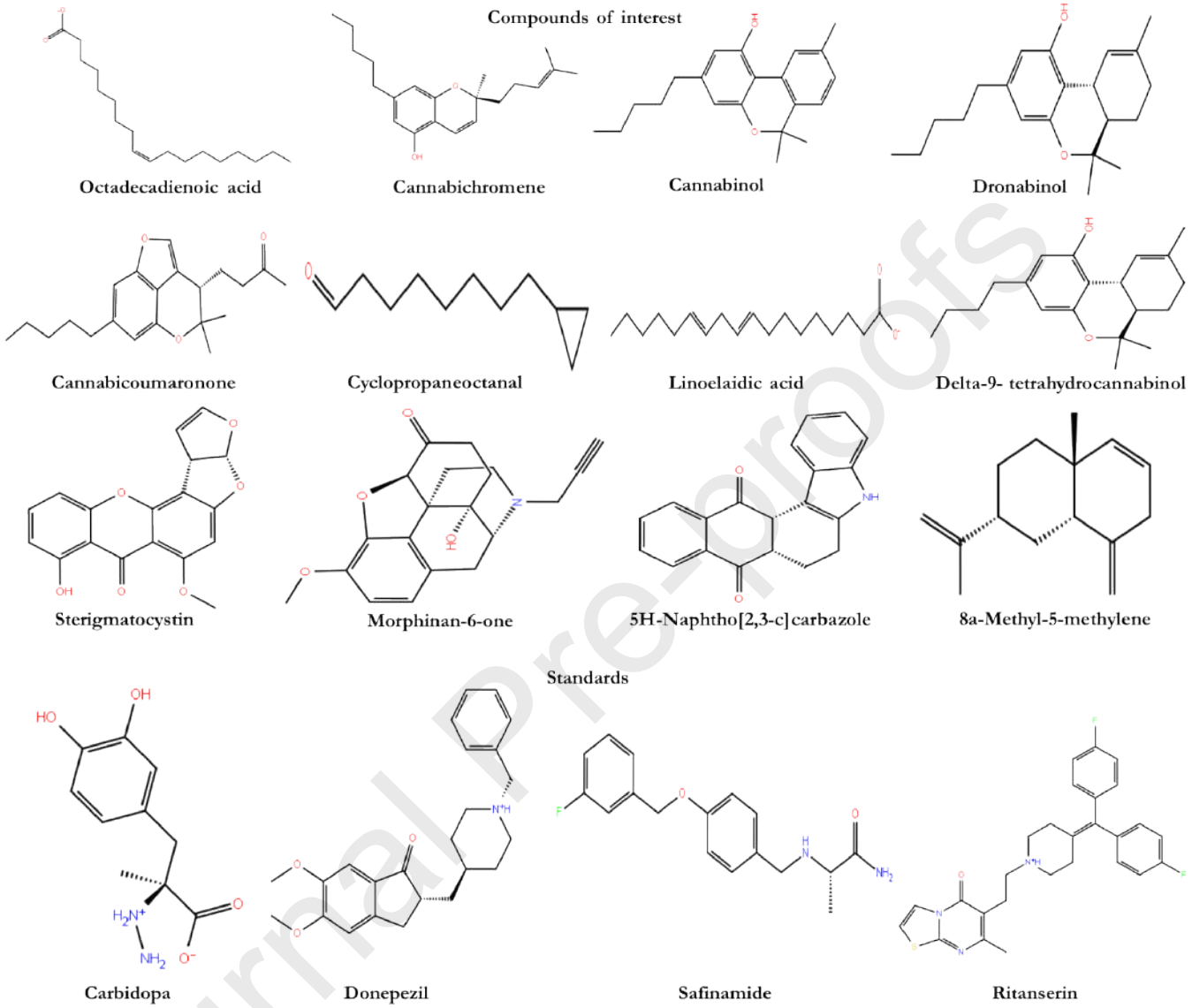

Figure 2: 2D structures of the studied ligands

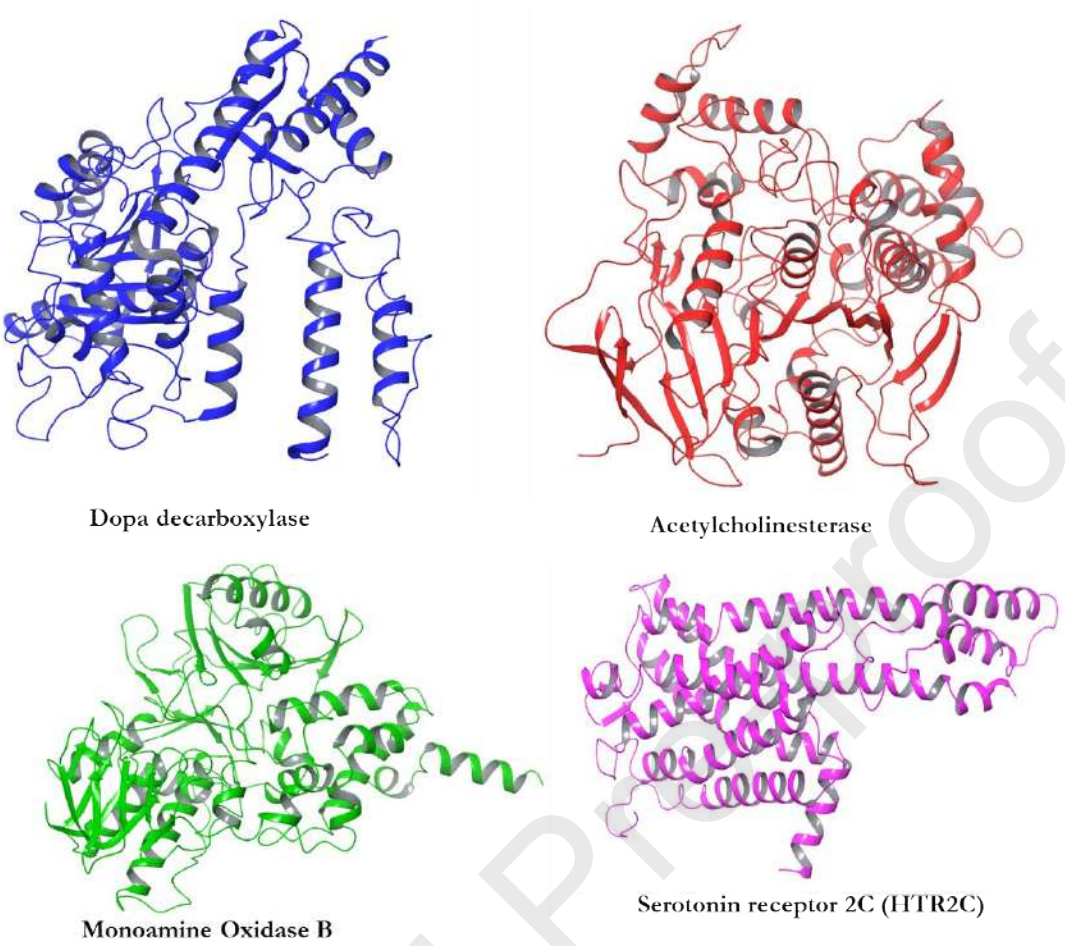

Figure 3: 3D structures of protein targets

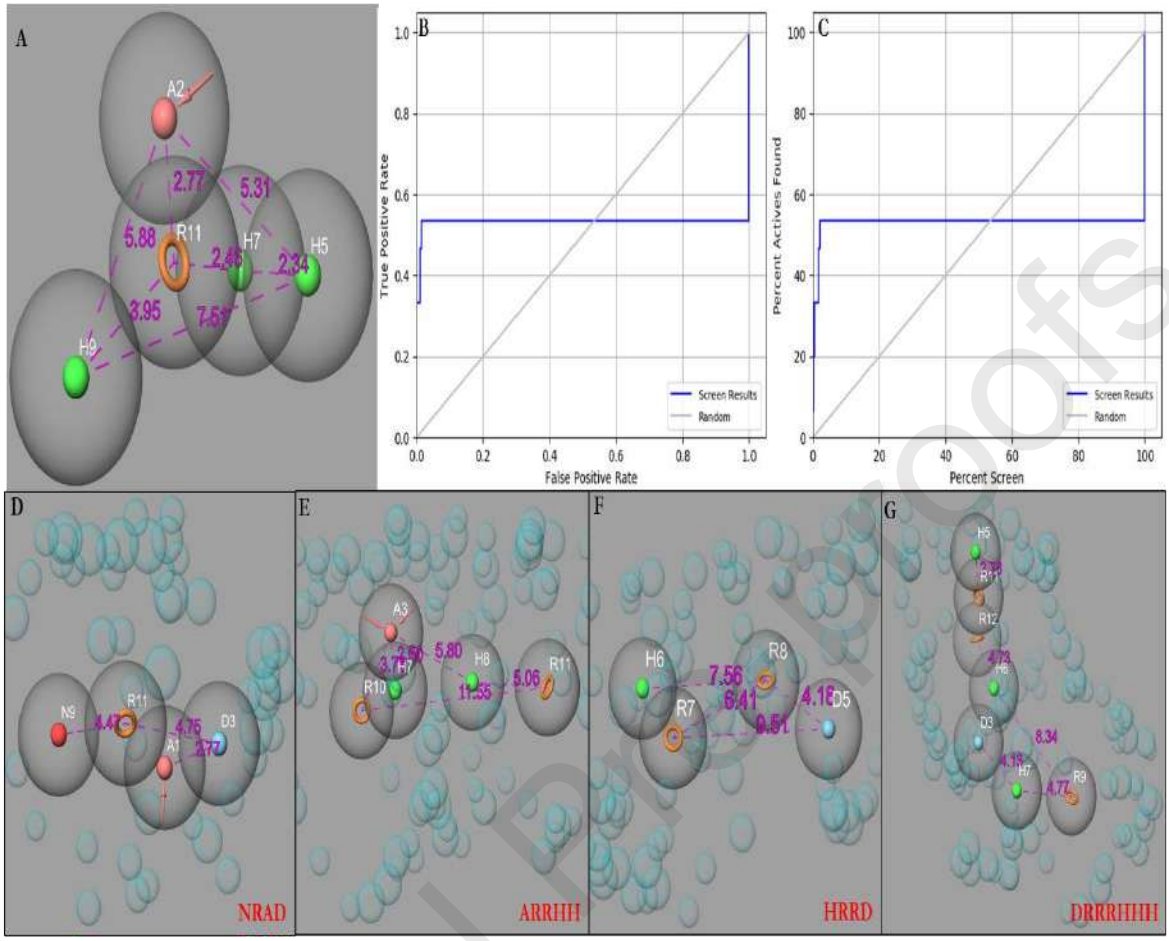

Figure 4: Pharmacophore hypothesis of the ligands A) The pharmacophore features AHHHR, B) The Receiver operating characteristic (ROC), and C) the percentage scoring result, D) Dopa decarboxylase receptor complex, E) acetylcholinesterase receptor complex, F) monoamine oxidase receptor complex, G) Serotonin receptor complex.

ACETYLCHOLINESTERASE

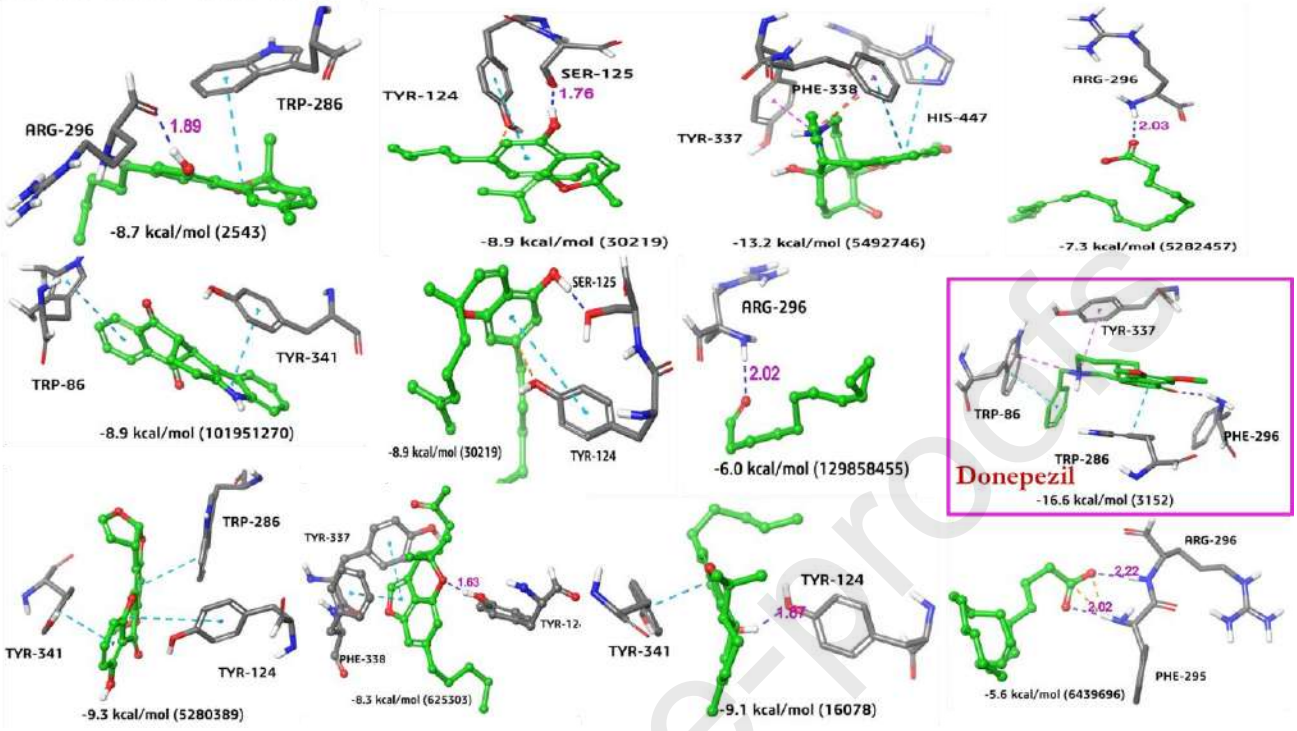

DOPA DECARBOXYLASE

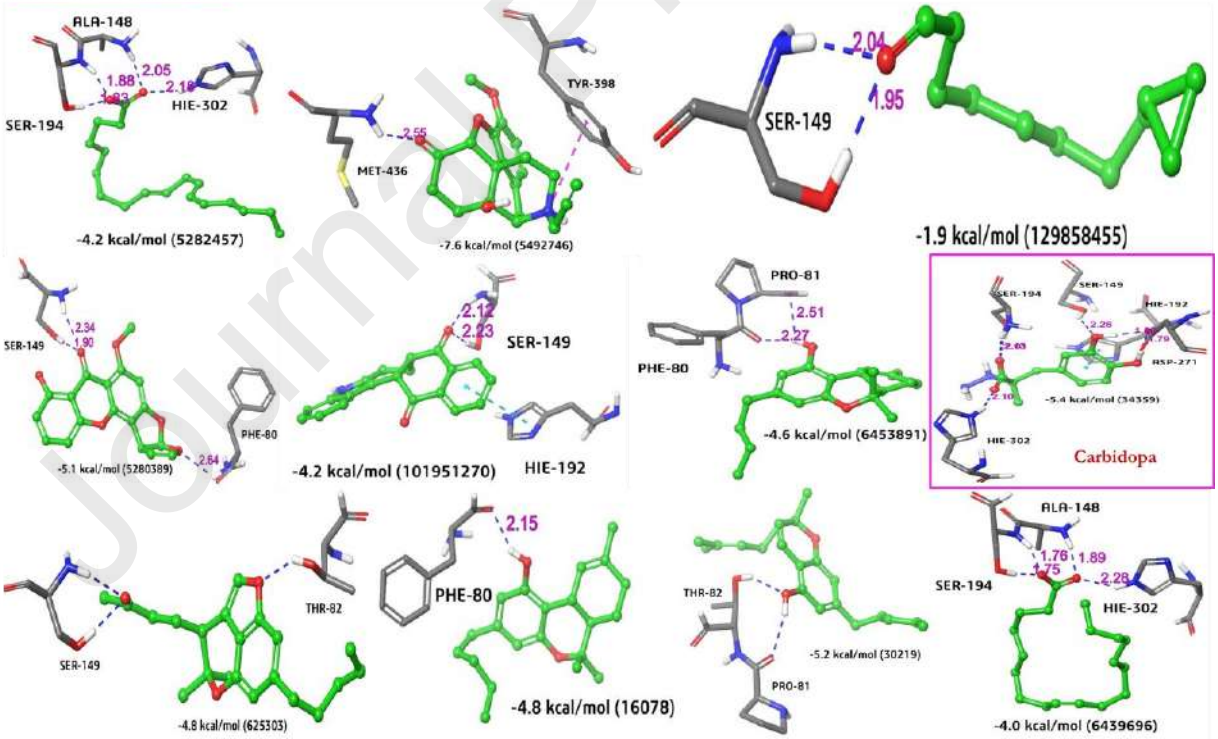

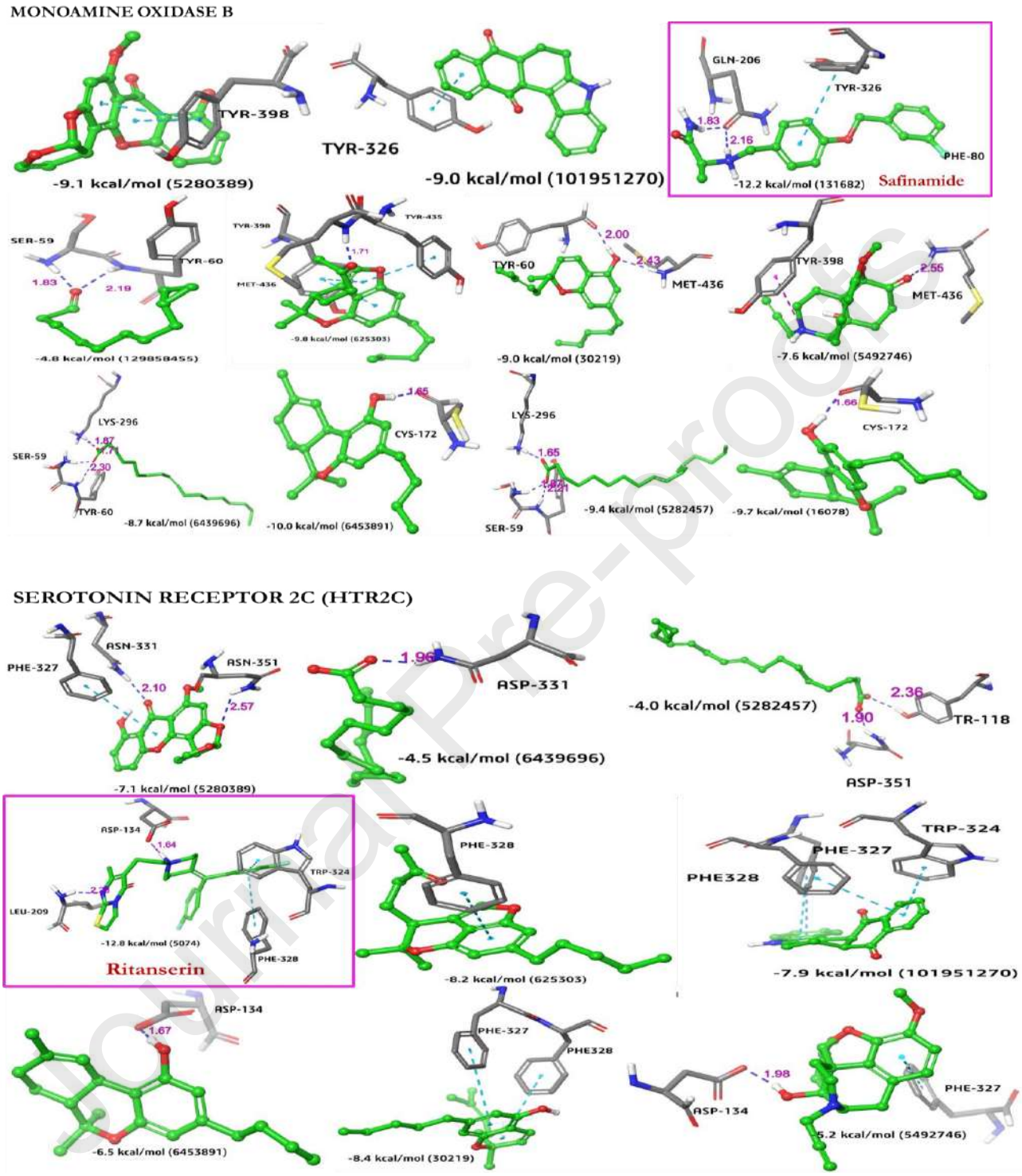

Figure 5: Molecular docking of compounds and standards

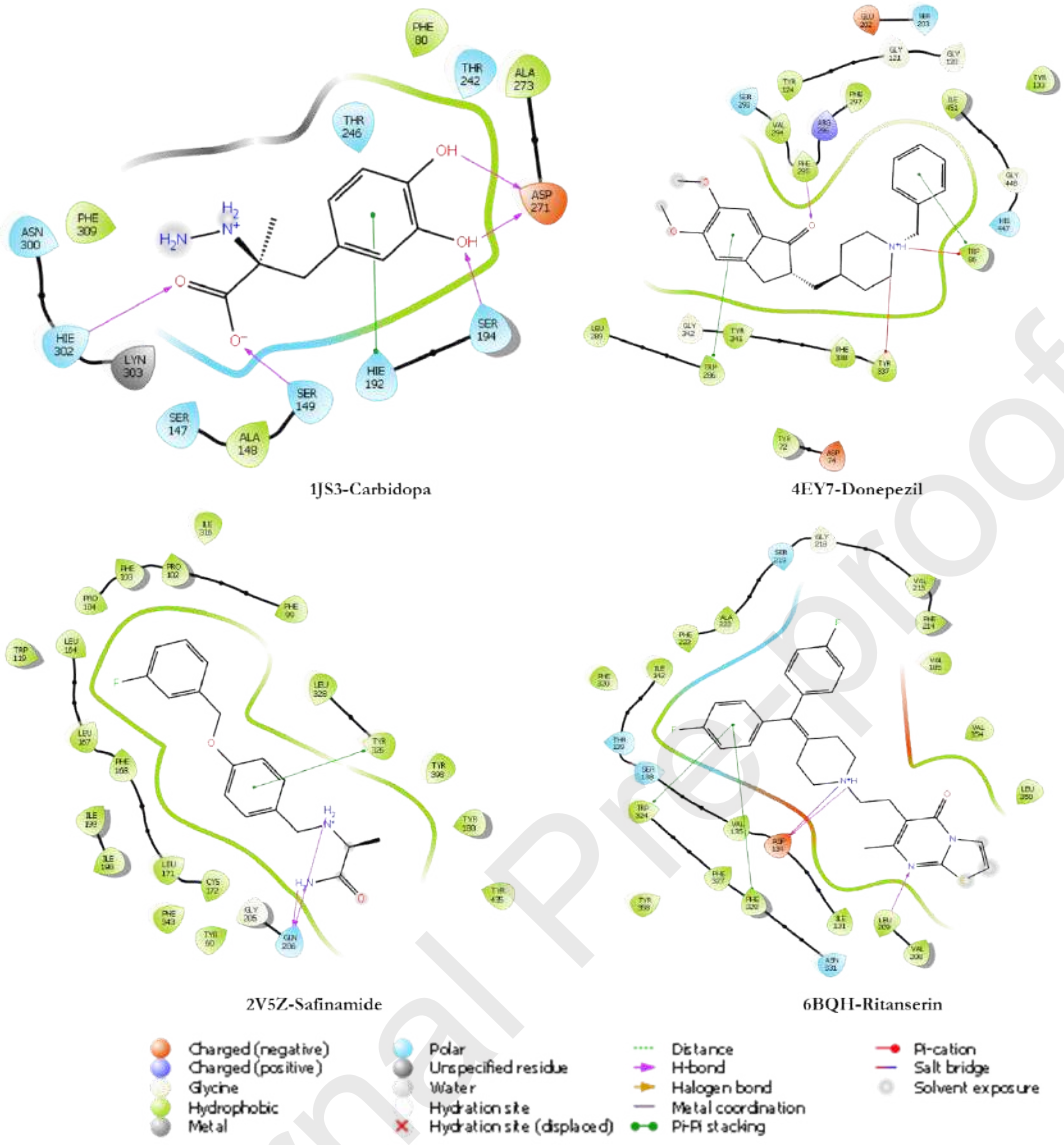

Figure 6: 2D-residue interaction of the standard ligands and their respective receptors.

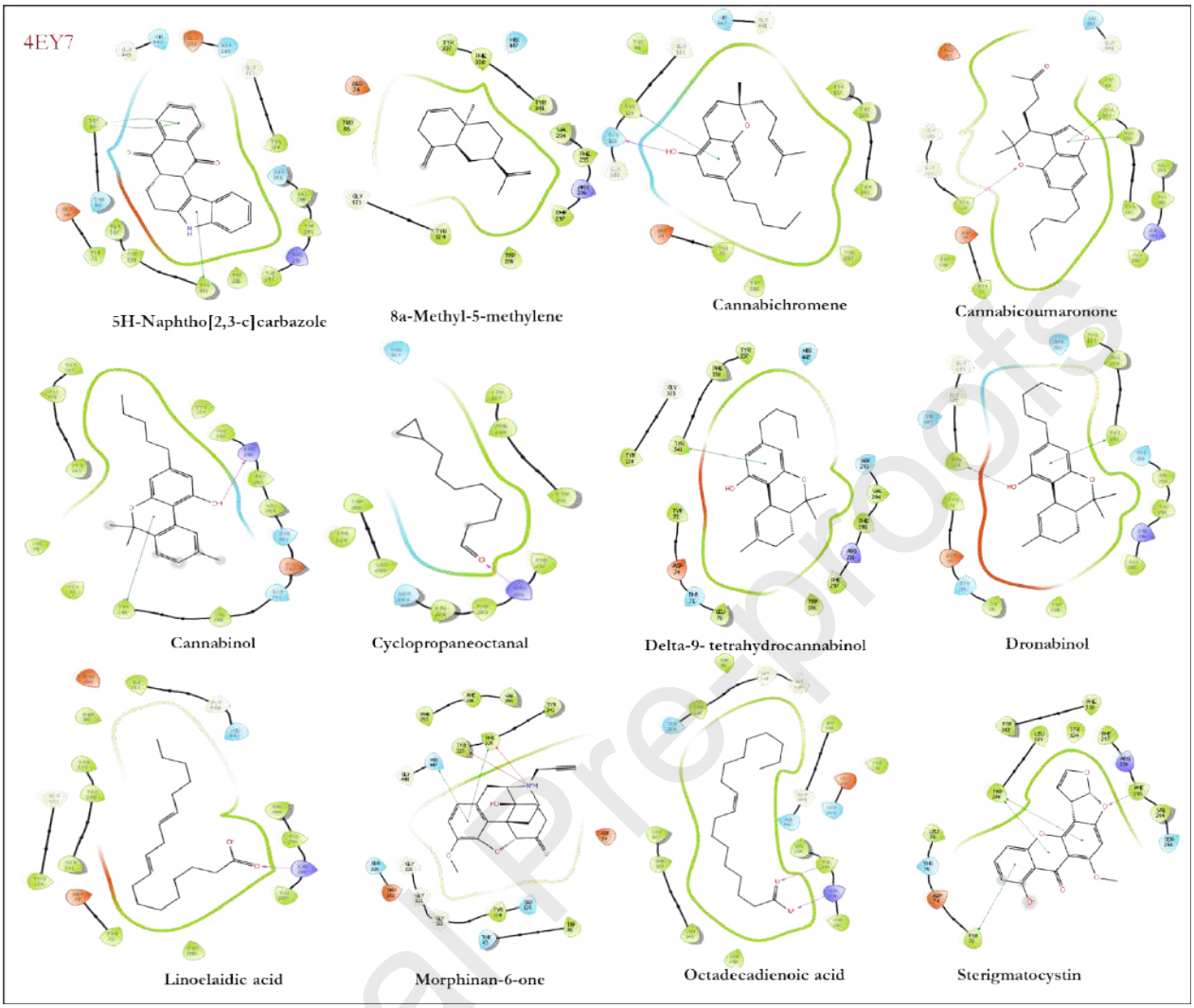

Figure 7: 2D-Ligand-receptor interactions observed after docking of compounds with acetylcholinesterase

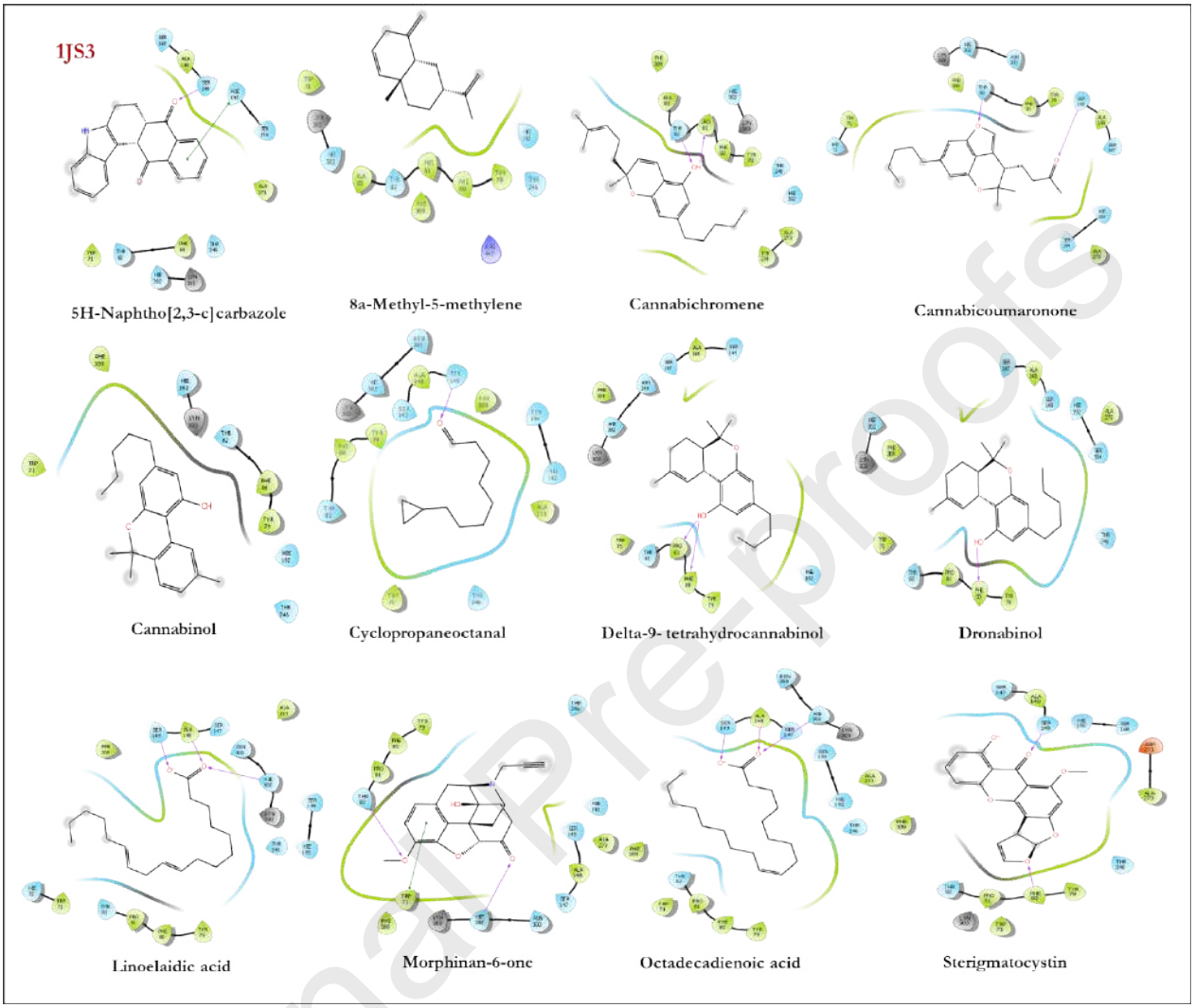

Figure 8: 2D-Ligand-receptor interactions observed after docking of compounds with dopa decarboxylase (DCC) gene

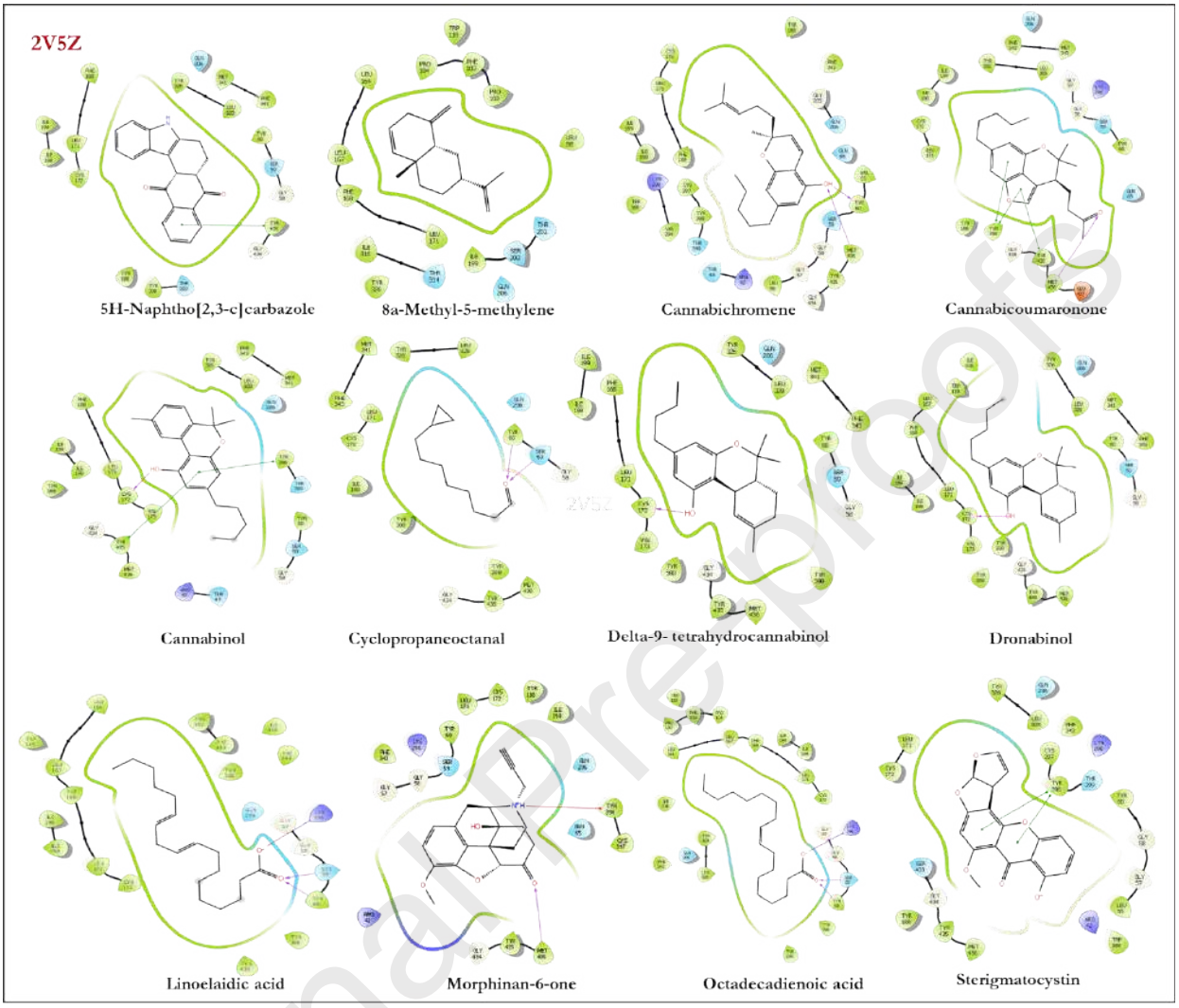

Figure 9: 2D-Ligand-receptor interactions observed after docking of compounds with monoamine oxidase (MAO)

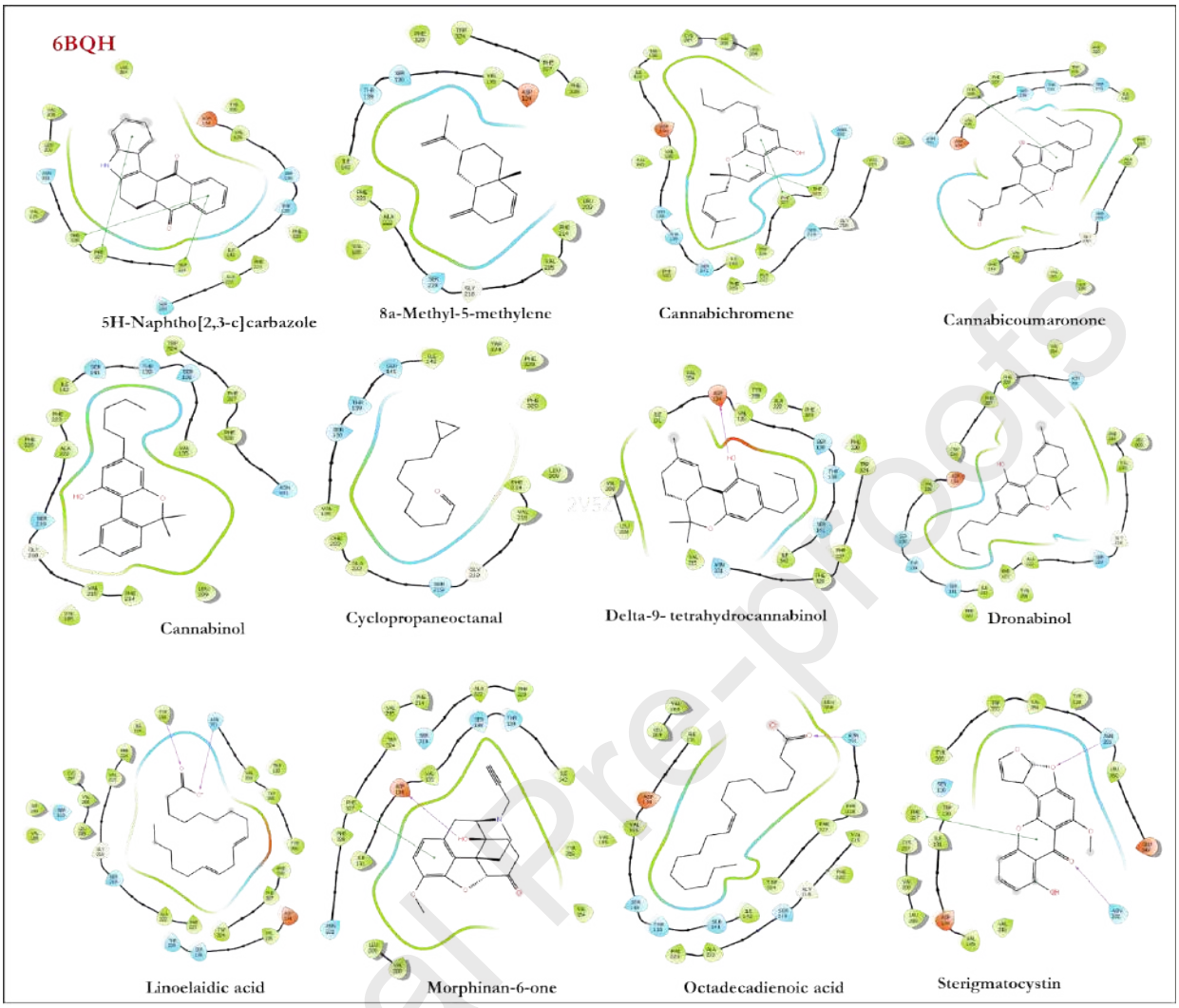

Figure 10: 2D-Ligand-receptor interactions observed after docking of compounds with serotonin receptor 2C (HTR2C)

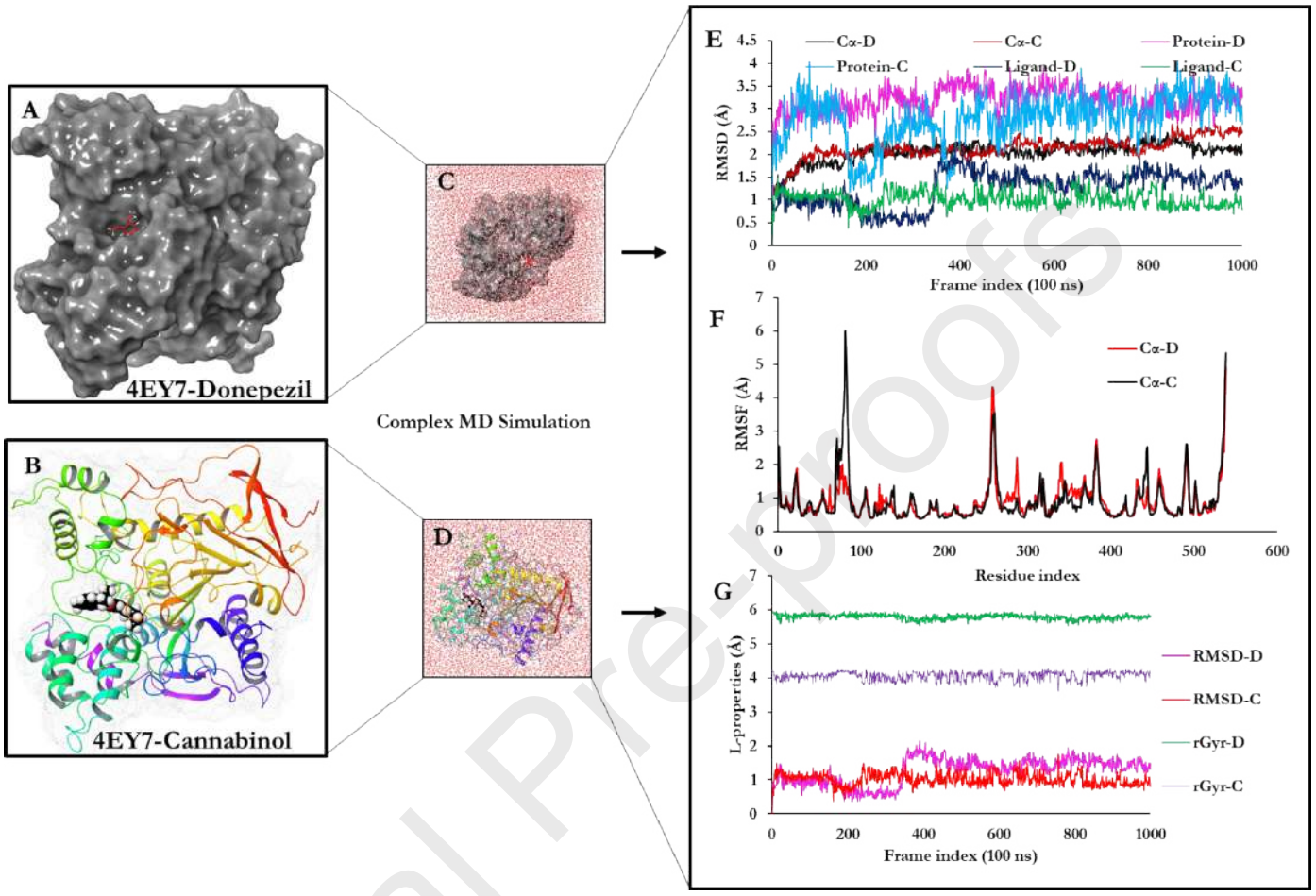

Figure 11: MDs analysis of AChE with donepezil and cannabinol over a frame index of 100 ns. A) System set-up for the simulation of AChE and donepezil, B) system setup for AChE -cannabinol complex, C the AChE -donepezil complex placed in a cubic box in the water system, D. the AChE -cannabinol complex placed in a cubic box in the water system, E. the RMSD of donepezil and Cannabinol in the receptor cavity, F. The RMSF of donepezil and Cannabinol in the receptor cavity. G. Ligand properties of donepezil and Cannabinol. Note: RMSD; Root Mean Square Deviation; RMSF: Root Mean Square Fluctuation

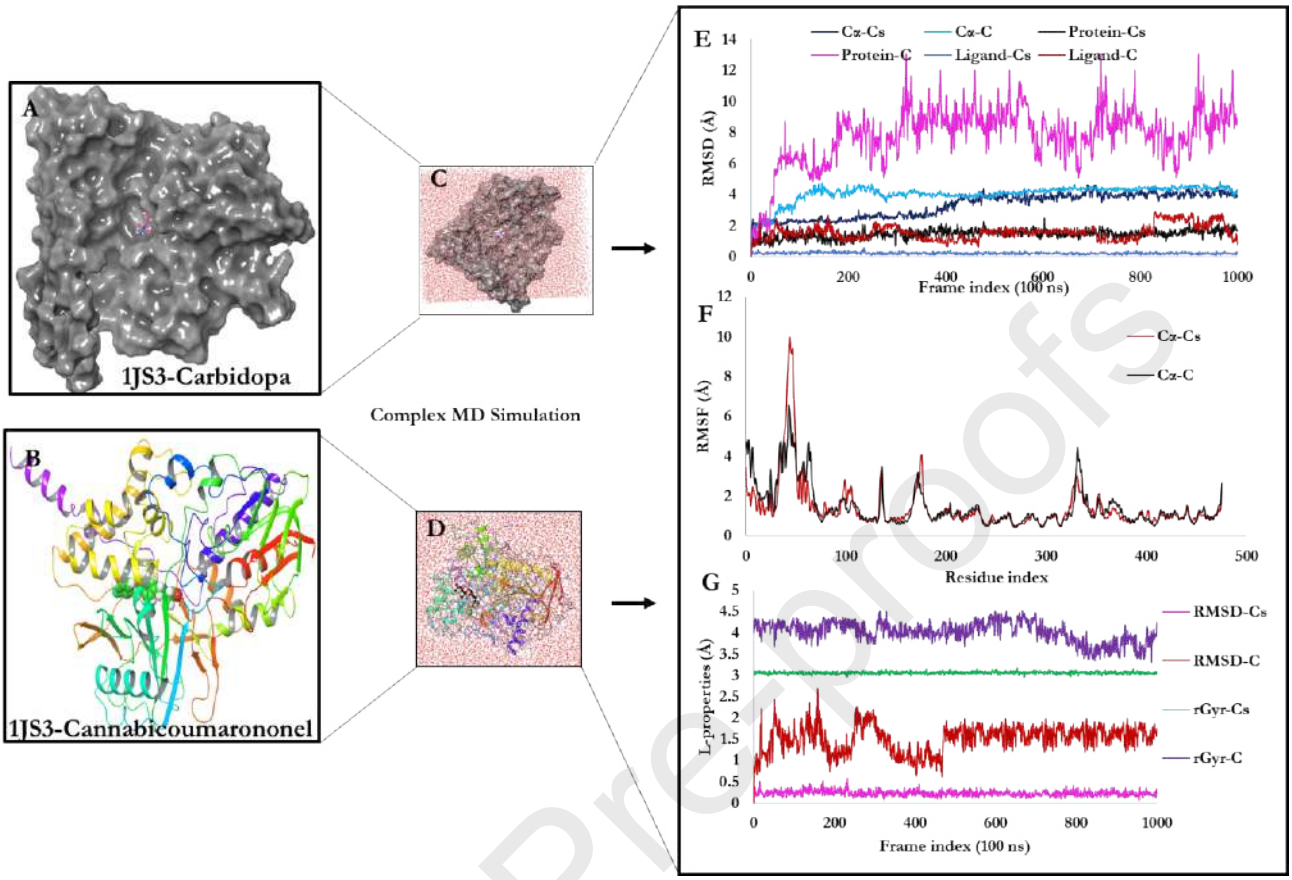

Figure 12: MDs analysis of DCC with carbidopa and Cannabicoumaronone over a frame index of 100 ns. A) System set-up for the simulation of DCC and carbidopa, B) system setup for DCC -cannabinol complex, C the DCC -carbidopa complex placed in a cubic box in the water system, D. the DCC -Cannabicoumaronone complex placed in a cubic box in the water system, E. the RMSD of carbidopa and Cannabicoumaronone in the receptor cavity, F. The RMSF of carbidopa and Cannabicoumaronone in the receptor cavity, G. Ligand properties of carbidopa and Cannabicoumaronone. Note: RMSD; Root Mean Square Deviation; RMSF: Root Mean Square Fluctuation

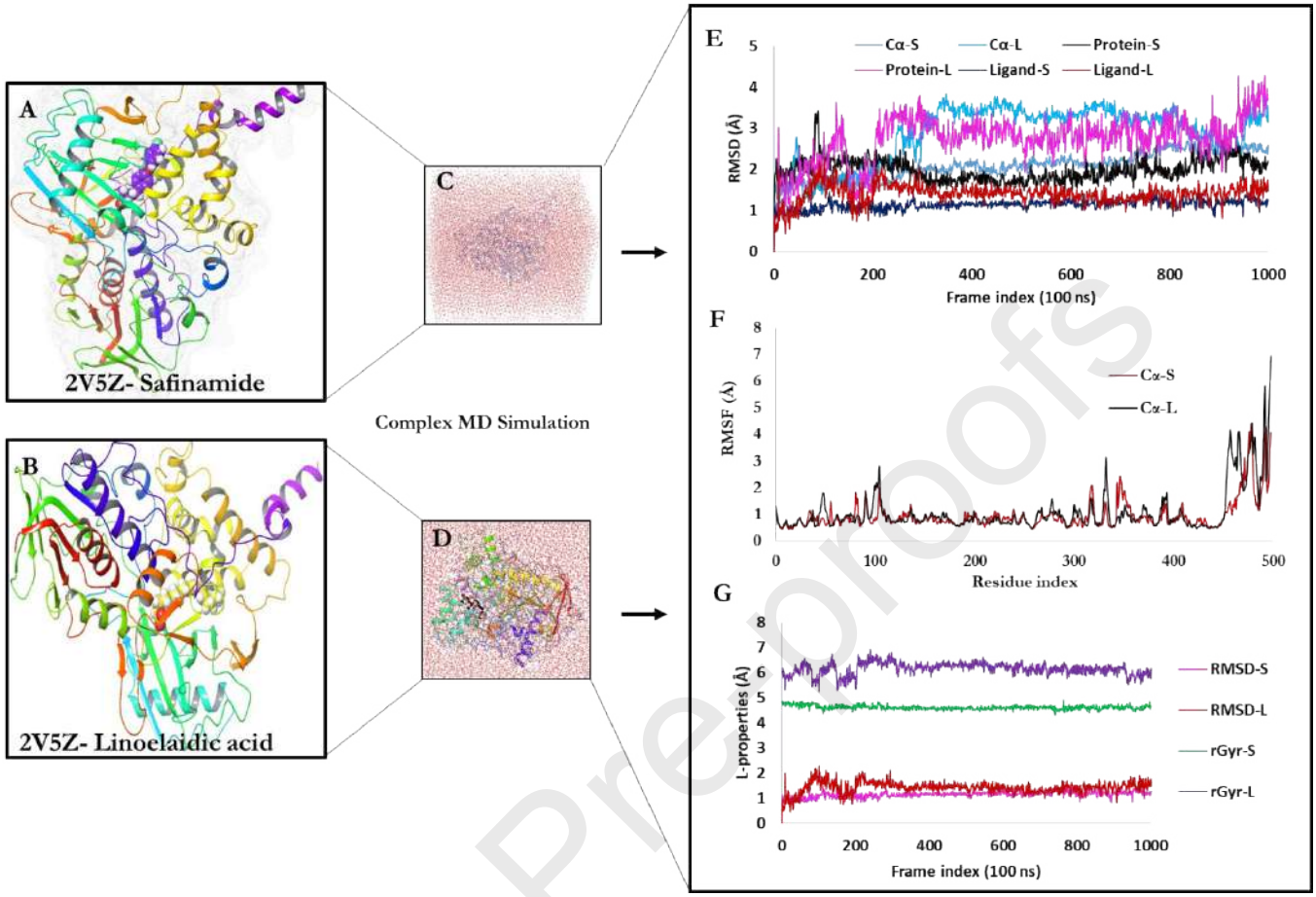

Figure 13: MDs analysis of MAO with safinamide and Linoelaidic acid over a frame index of 100 ns. A) System set-up for the simulation of MAO and safinamide, B) system setup for MAO-Linoelaidic acid complex, C the MAO-safinamide complex placed in a cubic box in the water system, D. the MAO-Linoelaidic acid complex placed in a cubic box in the water system, E. the RMSD of safinamide and Linoelaidic acid in the receptor cavity, F. The RMSF of safinamide and Linoelaidic acid in the receptor cavity, G. Ligand properties of safinamide and Linoelaidic acid. Note: RMSD; Root Mean Square Deviation; RMSF: Root Mean Square Fluctuation

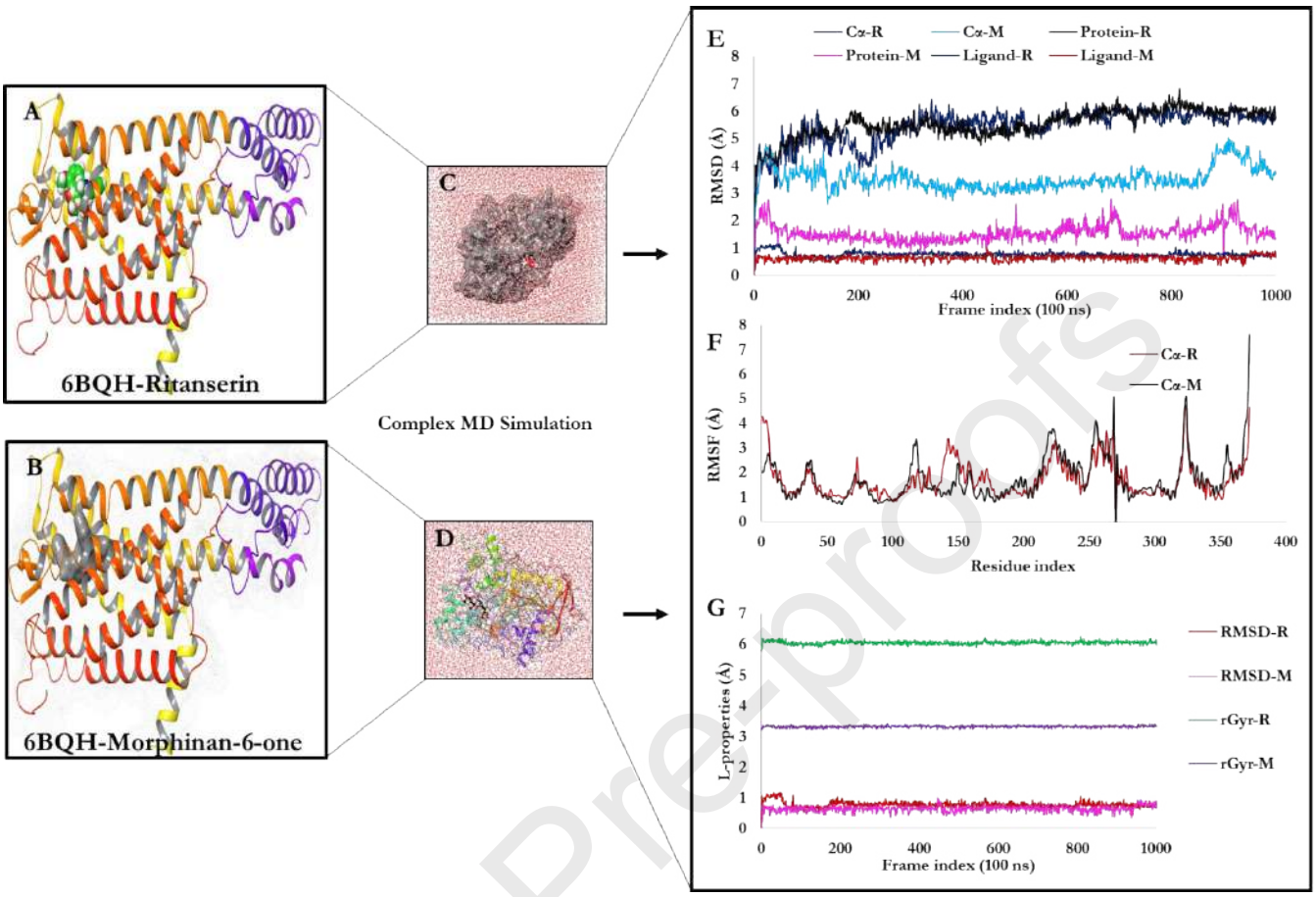

Figure 14: MDs analysis of HTR2C with Ritanserin and morphinan-6one over a frame index of 100 ns. A) System set-up for the simulation of HTR2C and Ritanserin, B) system setup for HTR2C-morphinan-6-one complex, C the HTR2C-Ritanserin complex placed in a cubic box in the water system, D. the HTR2C- morphinan-6-one complex placed in a cubic box in the water system, E. the RMSD of Ritanserin and morphinan-6-one in the receptor cavity, F. The RMSF of Ritanserin and morphinan-6-one in the receptor cavity of HTR2C, G. Ligand properties of Ritanserin and morphinan-6-one. Note: RMSD; Root Mean Square Deviation; RMSF: Root Mean Square Fluctuation